# Studies of Mixed-Anion Manganites and Other Compounds

by

Anita Dasu

Submitted in Partial Fulfillment of the Requirements

for the Degree of

Master of Science

in the

Chemistry

Program

YOUNGSTOWN STATE UNIVERSITY

August, 2008

**Studies of Mixed-Anion Manganites and Other Compounds**

by

Anita Dasu

I hereby release this thesis to the public. I understand that this thesis will be made available from the OhioLINK ETD Center and the Maag Library Circulation Desk for public access. I also authorize the University or other individuals to make copies of this thesis as needed for scholarly research.

Signature:

_____

Anita Dasu, Student Date

Approvals:

_____

Dr. Timothy R. Wagner, Thesis Advisor Date

_____

Dr. Sherri Lovelace-Cameron, Committee Member Date

_____

Dr. Brian D. Leskiw, Committee Member Date

_____

Dr. Peter J. Kasvinsky, Dean, School of Graduate Studies & Research Date

## ABSTRACT

Relative to oxides, mixed anion materials containing N and/or F dissolved within an oxide lattice offer a variety of advantages, including smaller band gaps and incorporating a greater variety of potential cations with a larger possible range of oxidation states. These factors, coupled with the relatively lowered symmetry that may occur due to anion ordering suggest enhanced dielectric, magnetic, and/or optical properties for the targeted materials. The goal of this project is to synthesize a mixed-anion analog of (Ca, La)$MnO_3$, which is well known for colossal magnetoresistive properties due in part to the presence of both $Mn^{3+}$ and $Mn^{4+}$ in the lattice. Such materials may have potential applications in magnetic storage devices (e.g. computer hard drives). Whereas the presence of mixed $Mn^{3+/4+}$ ions results from substituting $La^{3+}$ for some $Ca^{2+}$in the oxide lattice, the same effect can hypothetically be achieved through anion substitutions such as $N^{3-}$ and/or $F^-$ for $O^{2-}$. Attempts were made in this study to directly synthesize novel $CaMnN_xO_yF_z$ materials from binary Mn and Ca compounds, or from redox reactions in $N_2$, but they were unsuccessful. These attempts will be summarized and a new approach involving ammonolysis of $CaMnO_3$, followed by fluorination of the product to give the novel compound $Ca_2(Mn^{3+}, Mn^{4+})O_5F$, will be discussed.

A second project will also be discussed involving crystal chemical studies of $Sr_2BiGa_{11}O_{20}$. The single crystal X-ray structure of the compound, which is found to be isostructural with $Ba_2BiGa_{11}O_{20}$, is presented for the first time. The structure will also be discussed in the context of a bond-valence sum analysis.

## ACKNOWLEDGEMENTS

First and foremost, I thank my advisor Dr. Tim Wagner for all his time, patience, and insight these past two years. Without his guidance, none of the work in this thesis would be possible. I'd also like to thank my thesis committee members Dr. Brian Leskiw and Dr. Sherri Lovelace-Cameron for generously giving their time to critique this work. I wish to thank Dr. Matthias Zeller for his expertise and guidance in crystallography. I would like to thank the entire Chemistry Department at YSU for providing a learning environment that has allowed me to grow as both a scientist and a person.

Also, I thank Susan Achburger, a friend pursuing a Master's degree in biochemistry at Michigan State, for sharing the rewards and stress of this experience even from hundreds of miles away. I wish to thank Kat Pavlidakey, a fellow classmate here at YSU for keeping me company on many late nights while I was writing this thesis. I thank rest of my fellow graduate students for keeping me motivated throughout this academic endeavor.

Finally, I would like to thank my family for supporting me in all of my decisions and for always encouraging me to further my education. Most of all, I thank them for being there to help me, no matter what kind of trouble I got myself into. I love you.

# TABLE OF CONTENTS

**PAGE**

# LIST OF EQUATIONS

**EQUATION** **PAGE**

# LIST OF FIGURES

# LIST OF TABLES

**TABLE** **PAGE**

# CHAPTER 1

# INTRODUCTION

Solid-state chemistry is a relatively small but important subdiscipline of chemistry that plays a role in the design and production of many electrical devices from the twentieth century due to its unique interaction with electrical, mechanical, and materials engineering. Solid-state chemistry is the study of solid (usually crystalline) substances, and generally concerns the synthesis, structural characterization, physical properties, and applications of novel materials.[1] Such materials can be useful in the design and production of commercial devices due to their electrical, thermal, and magnetic properties. Perhaps the greatest challenge in solid-state chemistry is the lack of definitive rules to guide in the synthesis of novel materials. Common characterization techniques for solid materials include X-ray diffraction, Transmission and Scanning Electron Microscopy (TEM & SEM), and synchrotron diffraction. Novel materials may be further characterized by methods such as UV/VIS spectra or neutron diffraction. Since powder and single crystal X-ray diffraction were the only two characterization techniques utilized in this research, they will be the only methods discussed.

## X-ray Crystallography and X-ray Diffraction

X-ray crystallography is the preferred method of structure determination of crystalline materials. For small molecules, it simply compliments the use of spectroscopic techniques. It is however, the most important technique for structure determination in non-molecular materials.[2]

X-rays are part of the electromagnetic spectrum found between gamma and ultraviolet rays. They can be produced when high energy electrons ionize the 1s electrons

of a metal target; relaxation occurs as the electrons from 2p or 3p immediately drop down to the empty 1s level resulting in X-ray radiation characteristic of the metal target. Kα energy is produced when the electrons drop from 2p to 1s. Kβ energy is produced when the electrons drop from 3p to 1s.[3]

William Lawrence Bragg developed an equation that could accurately interpret the diffraction of crystals. He proposed the crystals are "built up in layers or planes such that each acts as a semi-transparent mirror."[2] Bragg demonstrated that the cleavage faces of crystals appear to reflect X-ray beams at a certain angle of incidence, θ, where the angle of incidence is also known as the *Bragg angle*. The Bragg equation is shown in **Equation 1.1**.

$$2d\sin\theta = n\lambda \qquad \textbf{Eq. 1.1}$$

The variable d is the perpendicular distance between the atomic layers in the crystal, or the d-spacing. The order of diffraction, n, could be any integer; λ is the wavelength of the incident X-ray beam. As illustrated in **Figure 1.1**, the incident angle of X-rays is equal to the angle of reflection of the X-rays.

The crystal planes from which X-rays diffract are described by integers (h, k, l). The terms for (h, k, l) are called Miller indices and their reciprocals represent the fractions along the three crystallographic axes that a crystal plane intersects. Miller indices are used to define all possible crystal planes that a certain crystal can contain. The relationship demonstrated in the Bragg equation requires that the phase of the reflected beam is equal in phase to the incident X-ray beam. Consider two X-ray beams, A and A', are reflected from adjacent planes B and B' within a crystal as shown in **Figure 1.1**.

When Bragg's law is obeyed, the reflected X-rays are in phase and interfere constructively; when the angle of incidence is anything other than the Bragg angle for this set of planes, the reflected rays are out of phase and interfere destructively.

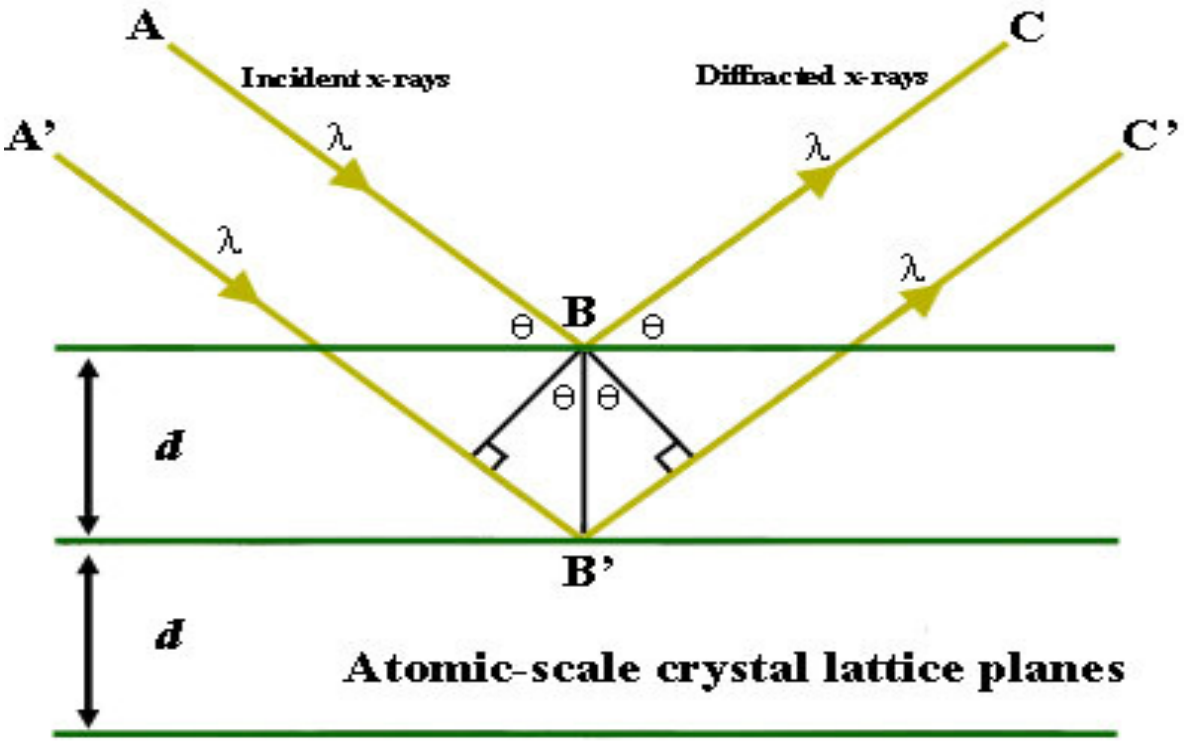


**Figure 1.1** Depiction of constructive interference of scattered X-rays in accordance with Bragg's Law.[4]

There are however, some limitations to Bragg's law. First, no information regarding the X-ray diffraction intensities is included in the equation, and this information is necessary for determination of an unknown crystal structure. Secondly, Bragg's law gives no indication of systematic absences in structures, which are reflections for which the intensity of the diffracted beam is zero. Systematic absences tend to arise when the lattice type is non-primitive, or from the presence of glide planes

and screw axes, and so are important in deducing the symmetry in a crystal. Lastly, Bragg's law doesn't explain the physics of diffraction or the interactions between electron clouds of atoms in crystals and incident X-rays.[2]

Powder and single crystal X-ray diffraction are two of the major characterization techniques used to determine the structure of crystals. An advantage of powder diffraction over single crystal X-ray diffraction is the relative ease of sample preparation, and in fact for some solid state reactions it may not be possible to obtain single crystals at all. Although powder diffraction can be used for quantitative structure determination, this is difficult relative to single crystal X-ray diffraction due to problems with peak overlap and multiplicity inherent in powder data. The most common use of powder diffraction is the qualitative identification of crystalline phases or compounds. Another advantage of powder diffraction is the ability to analyze mixed phases.

Single crystal X-ray diffraction is the preferred method of crystal structure determination. As mentioned, the preparation of suitable single crystal samples for X-ray diffraction is much more difficult than powder samples. Even if a single crystal is found, it may not be truly single crystalline and thus it may not be possible to determine the structure. Fortunately, advances in crystallographic software have made this less of a problem. Structure determination depends on the amount and quality of high intensity data, which is dependent on identities and relative positions of atoms present. A large amount of high intensity data is necessary to refine the data to a reliable structure. In general, structures with lower symmetry tend to have a larger number of variables.

In the present study, air sensitive materials are mixed in petroleum jelly on a glass slide and mounted on the goniometer head. All single crystal data presented herein was

collected on-site at YSU. The crystals are usually small and have to be mounted on a capillary tube and protected from air when bombarded by X-rays. If the crystal is larger than the X-ray beam, absorption becomes a problem. If the crystal is smaller than the beam, there may not be enough data to obtain sufficient intensities. This is a problem because solving the structure of an unknown crystal is dependent on the amount and quality of high intensity data collected. The process of solving a crystal structure is long and mathematically complex, but thanks to advances in software, most of the work is computer automated. West[2] compares solving an unknown structure to solving a set of simultaneous equations. There must be many more intensities than variables, as some of the intensity data may have errors. The intensity data is corrected for polarization factors and converted to observed structure factors, $F_{obs}$ The structure factors obtained are related to intensities by $F_{obs} = \sqrt{I_{obs}}$. While the magnitudes of $F_{obs}$ are determined, the phases are not. Phases are related to the atomic positions x, y, z, as seen in the equation $F_{obs} = |F_o| \exp[-i\alpha] = |F_o| \exp[-2\pi i(hx + ky + lz)]$, where $F_o$ = maximum amplitude and $\alpha$ is the phase. Also, $I_{obs}$ is positive and F can be either positive or negative. This leads to the inevitable phase problem. The phase problem arises because the phases cannot be determined directly from the intensities given. This problem can be solved either with direct or Patterson methods. Patterson methods use a Fourier summation to create a map with regions of high electron density corresponding to vectors between pairs of atoms. This method gives rise to peak heights of the largest atoms in the unit cell first, and once an atom is located, other atoms can be located through the Patterson map. Patterson methods work best when there are a small number of heavy atoms present.[3]

The other approach used to solve the phase problem is referred to as 'direct methods', which utilizes statistical probabilities to assign phases as being + or − for centrosymmetric structures, or being within a certain quadrant for non-centrosymmetric cases. Phases are first assigned to a starting set of select reflections, including some that define the origin. The phases of other reflections are then assigned using triplet relationships, which involve sets of reflections for which the h, k, l's of two reflections sum to give the h, k, l of the third reflection in the set. If the phases obtained through these sets of triplet reflections are self-consistent, then the starting set is taken as correct and can used to obtain an E-map, which in turn can be to determine atomic positions. Once the structure is solved, it is refined using a least squares method until the experimental vs. refined intensities converge as closely as possible.

**Perovskites**

Perovskites are a class of crystalline solids that have the general structure $ABX_3$, where A is a larger metal ion such as Ca, B is a transition metal, and X is an anion. Perovskite itself is $CaTiO_3$, although many perovskite-like compositions are known. The ideal cubic perovskite structure is illustrated in **Figure 1.2**. For an ideal cubic perovskite structure, the equation below will be obeyed, where R represents the respective ionic radii:

$$\mathbf{R_x + R_A = 1.414(R_x + R_B)} \qquad \textbf{Eq. 1.2}$$

This equation assumes that all atoms are touching. The cell edge is given by $(2R_x + 2R_B)$, and R is the radius of O and B, respectively. The diagonal of the unit cell is 1.414 multiplied by the cell edge.

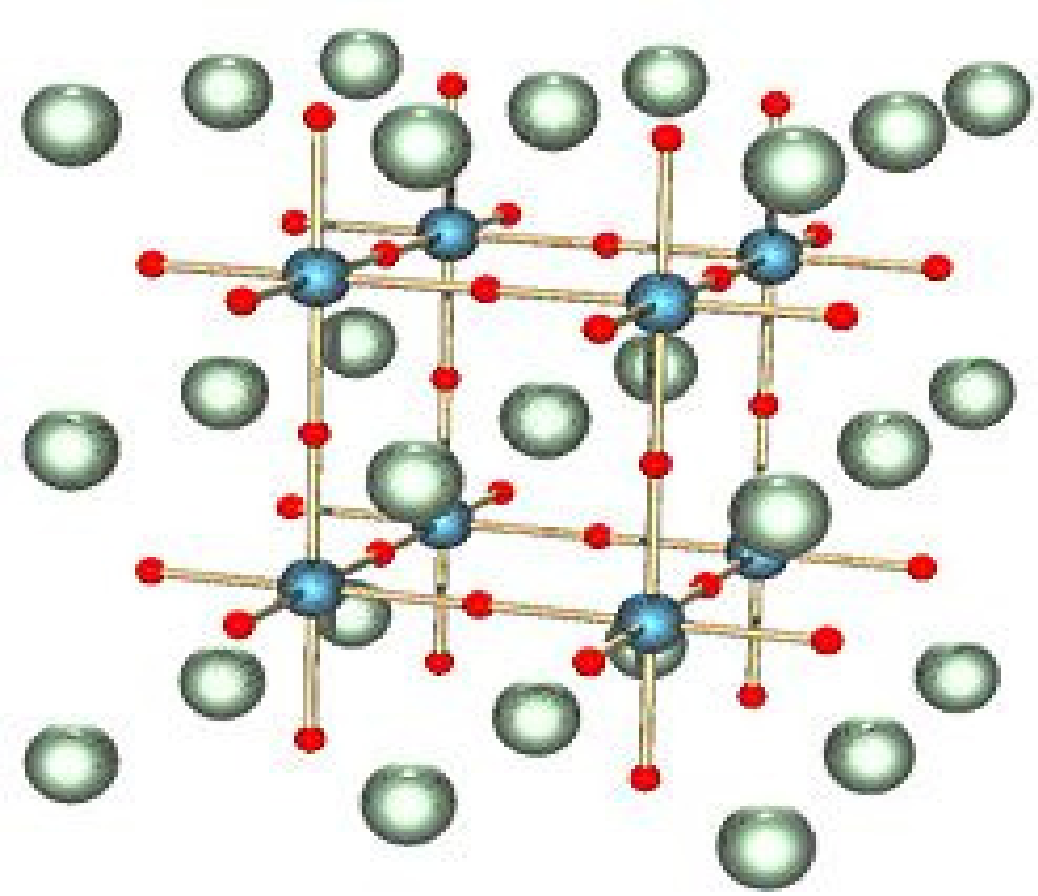

**Figure 1.2** Ideal cubic Perovskite Structure, $ABX_3$. Large green spheres are the A-type atoms in 12-fold coordination, blue spheres are the B-type atoms in octahedral coordination, and the red spheres are the X anions.[5]

Perovskite-related structures, however, are not always ideal and thus allow for a tolerance factor, *t,* to be applied to give the following equation.

$$R_x + R_A = t * 1.414(R_x + R_B) \qquad \textbf{Eq. 1.3}$$

The tolerance factor represents the degree of variation of radii of the atoms in the perovskite structure. In general, the tolerance factor for the perovskite structure is between 0.80 and 1.00. The ideal perovskite structure appears to only be possible in compounds with a tolerance factor between 0.90 and 1.00.[2] When a compound has a tolerance factor outside this range, it will adopt a deformed structure where the atoms are slightly displaced from their ideal positions, thus reducing the symmetry of the structure. As a result, many perovskites appear to have orthorhombic or monoclinic symmetry as opposed to the cubic symmetry of the ideal perovskite unit cell. The Ca/La manganites mentioned previously as being well known for their CMR behavior are examples of such perovskite-related materials, and are further discussed in the next section.

**Colossal Magnetoresistance**

Colossal magnetoresistance refers to a dramatic change in resistivity in the presence of a magnetic field. Thus, while conventional materials display about a 5% change in resistance in the presence of a magnetic field, CMR materials display a change by an order of magnitude. **Figure 1.3** illustrates CMR behavior in (La, Sr)$MnO_3$. This new phenomena was discovered in 1993 and cannot yet be explained theoretically.[6] Although the CMR effect is not well understood, one of several significant factors accounting for this behavior is thought to be strong electron-phonon coupling, which can

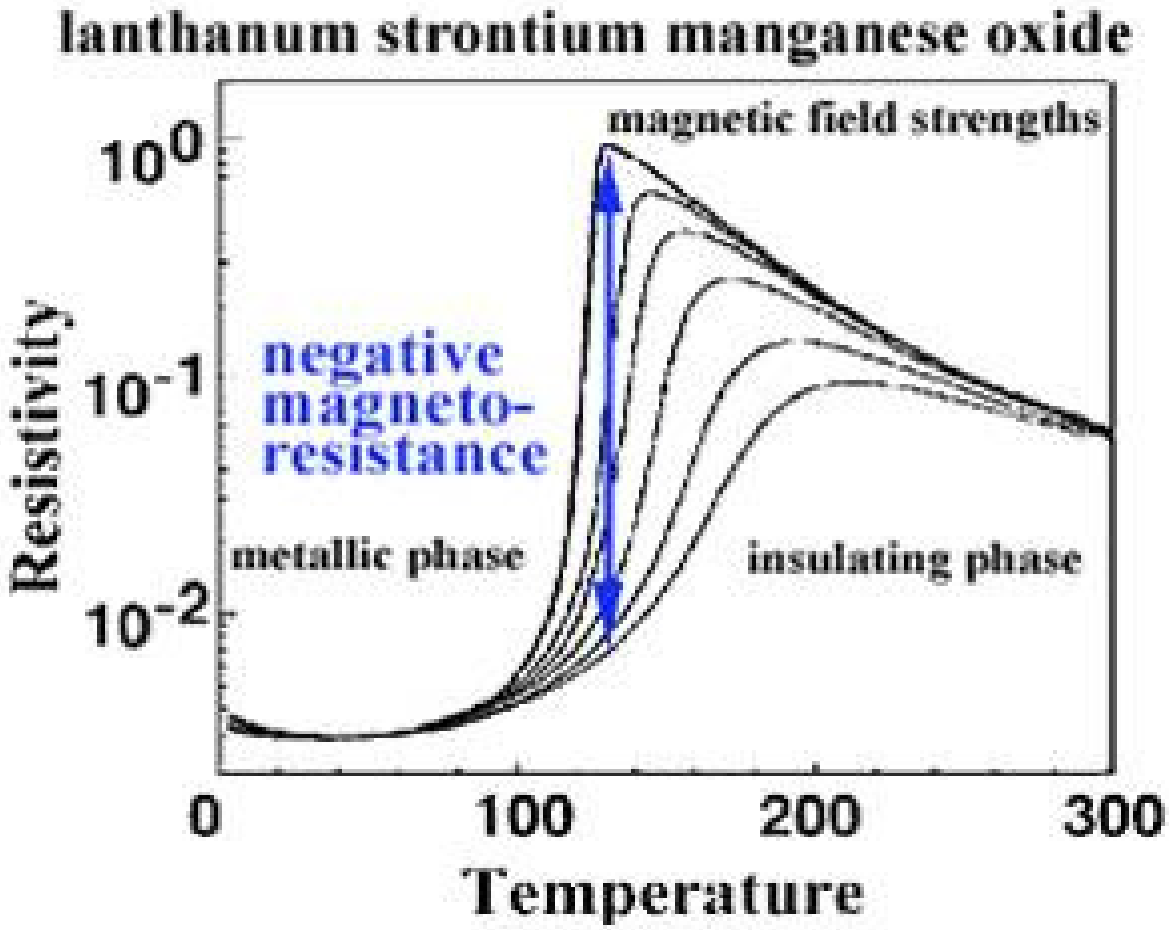


**Figure 1.3** Plot depicting CMR behavior for (La, Sr)$MnO_3$[9]

stem from a large Jahn-Teller effect.[7] For the family of compounds $[Ca_xLa_{1-x}][Mn_{1-x}^{3+}, Mn_x^{4+}]O_3$, CMR behavior is observed in the range ≅ 0.2-0.4.[7] Note that $Mn^{3+}$ is a $d^4$ ion for which Jahn-Teller distortions are expected while no Jahn-Teller distortions are expected in $Mn^{4+}$, a $d^3$ ion. Thus the presence of mixed oxidation states appears to give rise to CMR behavior in these materials.

Previous research suggests that most materials displaying CMR behavior do so under the action of the double exchange mechanism.[8] The double exchange mechanism

predicts the ease at which an electron may be exchanged between two species. It is a ferromagnetic exchange interaction between two atoms, meaning the electron spins remain aligned. As illustrated in **Figure 1.4**, double exchange is facilitated when the itinerant electron of the donor atom does not have to change spin and conforms to Hund's rule when moving to the acceptor atom. This reduces kinetic energy and the overall energy saved could lead to ferromagnetic behavior, resulting in easier conduction of electrons. **Figure 1.5** depicts the structure typical of La-doped manganite perovskites with CMR behavior. Chains of $Mn^{3+}$-O-$Mn^{4+}$ linkages required for double exchange occur along the b-axis. The double exchange mechanism is a guiding hypothesis for the work in this thesis, as all the mixed-anion target compounds are designed such that they contain both $Mn^{3+}$ and $Mn^{4+}$ ions.

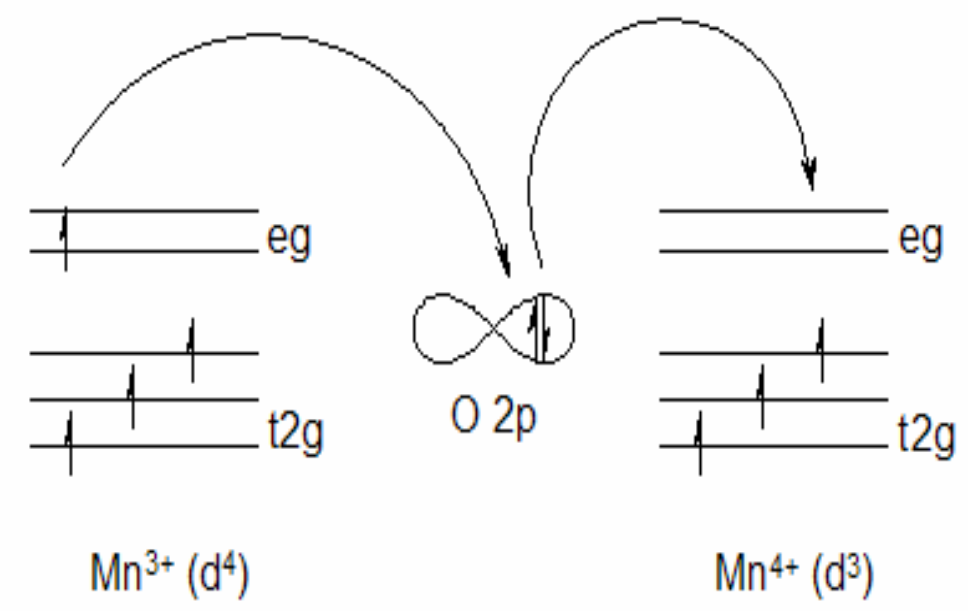


**Figure 1.4** Depiction of the Double Exchange Mechanism[10]

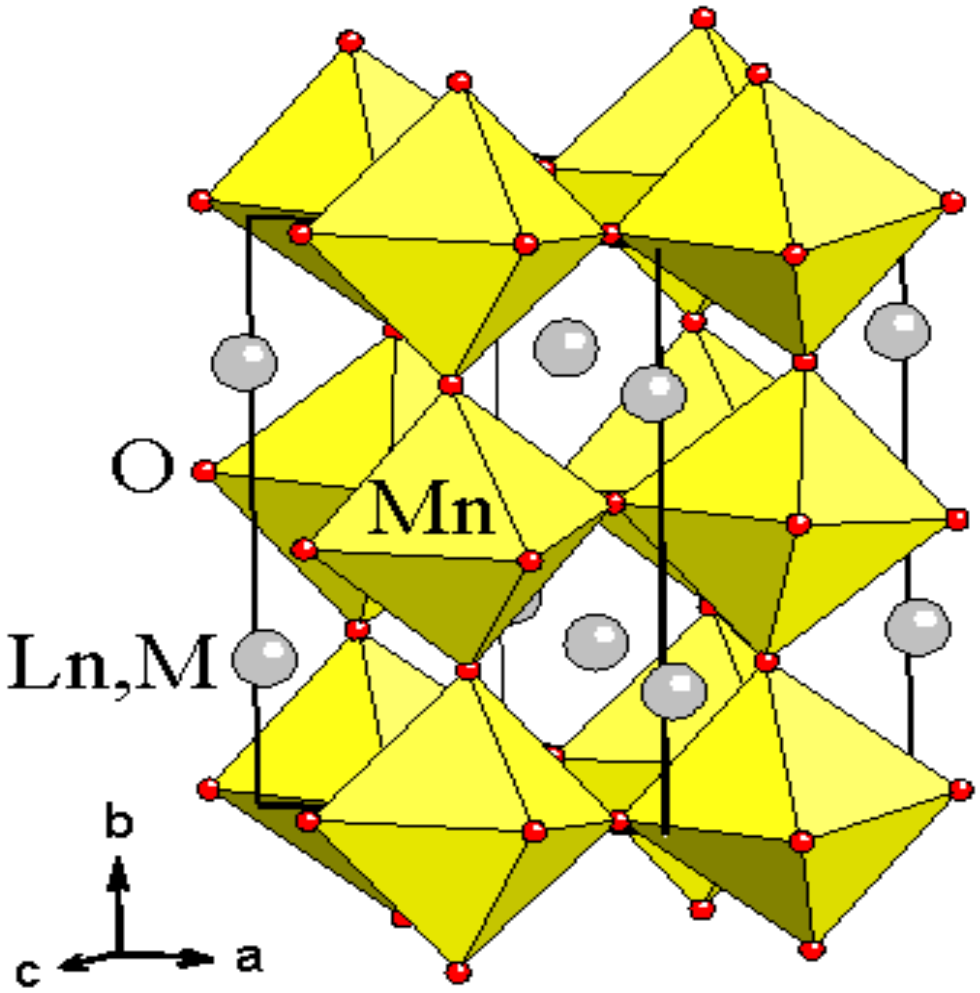


**Figure 1.5** Structure for perovskite-like (La, M)$MnO_3$ phases, where M = Ca or Sr; chains of $Mn^{3+}$-O-$Mn^{4+}$ linkages occur along the b-axis. For $CaMnO_3$, the lattice is orthorhombic with a= 5.262 Å, b=5.275 Å, c=7.448 Å.[11]

As stated earlier, perovskite-based compounds are of great technological importance due to their unique properties, including CMR, which is of interest in this research. CMR behavior is common in a family of double distorted perovskites with the general formula $AC_3B_4O_{12}$ where C is a cation displaying Jahn-Teller distortions (e.g. $Cu^{2+}$, $Mn^{3+}$), A is a cation of large radius (e.g. $Ca^{2+}$, $Na^{+}$, alkali-metal, alkaline-earth metal, or rare earth metal), and B is a cation of octahedral oxygen forming a metal structure skeleton.[12] The magnetoresistance of these compounds is comparable to $La_{1-x}A_xMnO_3$ pervoskites.

There have been relatively few research studies on metal N-O-F systems in general. Some papers have been published on fluorite-type compounds, including Zr-N-O-F[13], Ce-N-O-F[14] and In-N-O-F[15] systems. Danielle Jack synthesized a series of $TiN_xO_yF_z$ compounds for x very small (i.e. for $x < 0.1$), which varied in color from yellow to green apparently depending on the relative amounts of N and F doped into the $TiO_2$ lattice.[16] Considerable work has also been done elsewhere on nitrogen-doped $TiO_2$ and has confirmed that the presence of nitrogen is crucial to enhance these properties of $TiO_2$ by narrowing the band gap.[17] There are also several reports in the literature involving studies of oxynitride perovskites, which focus primarily on dielectric properties.[18]

# CHAPTER 2

## STATEMENT OF THE PROBLEM

The overall goal of this research is to create a mixed anion analog that is expected to display colossal magnetoresistant behavior as observed in La-doped $CaMnO_3$. The guiding hypothesis for this work is based on the premise that the double-exchange mechanism is an important criterion in CMR behavior. This requires the presence of mixed $Mn^{3+}/Mn^{4+}$ ions which we attempt to introduce in perovskite-related manganites through anion rather than cation substitution for the first time. The specific compositions having mixed $Mn^{3+/4+}$ ions targeted in this study are $Ca_2Mn_2O_4N$ and $Ca_2Mn_2O_5F$. Direct synthesis of the novel compounds from binary Mn and Ca compounds or from redox reactions in $N_2$ have yielded little success thus far. Therefore, alternative reaction routes have been explored and will be briefly discussed herein.

The existence of $SrBi_2Ga_{11}O_{20}$ has previously been reported but no quantitative structure determination has been published to date. The final chapter will discuss the structural characterization of this compound.

# CHAPTER 3

# MATERIALS AND METHODS

Most of the work presented in this thesis is concerned with the synthesis, sample preparation, and characterization of $Ca_2Mn_2O_4N$. This chapter will discuss the techniques used in the synthesis, along with powder and single crystal preparation methods.

## Oxynitride Synthesis

Several attempts to prepare $Ca_2Mn_2O_4N$ were made under a variety of reaction conditions. The synthetic preparations were always done under an inert atmosphere. Such an atmosphere was created in a sealed plastic glove bag filled with argon gas. Once the glove bag was filled with argon gas, the reactants were weighed and placed into a nickel crucible. The nickel cap was placed over the crucible containing the reactants and placed onto a nickel boat to stabilize the crucible during the reaction. The boat was then placed into a quartz reaction tube. The reaction tube was capped with a Pyrex tube and removed from the glove bad and placed inside the tube furnace. In order to prevent any leaks between the tube and the Pyrex cap, the cap and tube were secured using a copper wire.

A Thermolyne High Temperature Tube Furnace, Model 59300, was used for all reactions discussed in this thesis. For optimal heating, the reaction tube was inserted so that the crucible would be in the center of the furnace. The synthesis process is divided into five steps that were directly programmed into the furnace. For each step, three parameters were specified: the ramp rate, “R,” i.e. the rate of heating or cooling; the desired temperature level, “L,”; and the dwell time, “D,” which is the desired time to remain at specific temperature. The “Step Function” commands the furnace to heat or cool to the desired temperature as quickly as possible.

Once a reaction completed, the glove bag was again filled with argon gas to provide an inert atmosphere. The reaction tube was then removed from the furnace and placed into the glove bag, where the boat was removed from the reaction tube. A portion of the sample was usually placed onto a glass slide, and if the crystals were thought to be air sensitive, they were mixed with petroleum jelly to prevent any reaction with air. The glass slide was then removed from the glove bag and placed under a microscope so that any single crystals could be isolated with the use of a scalpel. An ideal single crystal is generally uniform in color and free of any black specs or white powders. If a specimen was thought to be single crystalline, it was mounted in a capillary tube or on a MiTeGen mesh micromount. X-ray data was collected on-site using a Bruker SMART APEX 4k CCD system. Refinement of data was accomplished using SHELTXL 6.14 software.

**Powder Sample Preparation**

Powder sample preparation for X-ray diffraction analysis is relatively simple compared to single crystal preparation. There are two modes in which the powder diffractometer can be set, reflective mode and capillary mode. Powder sample preparation depends on which mode the instrument is set up for. In reflective mode, the powder sample is packed tightly into a sample cup so that the top of the cup is level and evenly distributed. In capillary mode, the sample is preferably packed inside the capillary tube, although sometimes if the tubes were difficult to pack, the powder was dispersed on the outside of a tube and coated with petroleum jelly. Once the powder is packed on or coated in the capillary tube as evenly as possible, it is then mounted on a goniometer head. The powder X-ray diffraction patterns were collected at room temperature using a Bruker D8 ADVANCE Diffractometer. Every known crystal phase has a characteristic

powder pattern that can be used as a fingerprint to identify that compound, and these patterns are listed in a database. Our data was analyzed and fitted to the database patterns using the EVA Application software.

**Bond Valence Sum Theory**

The bond valence theory is an excellent tool for checking X-ray structures and is much more effective at predicting bond lengths in crystal systems than using the sums of ionic radii. Bond valences can be calculated using **Equation 3.1:**

$$\upsilon_{ij}=\exp[(R_{ij}-d_{ij})/b] \qquad \textbf{Eq 3.1}$$

The bond valence, $\upsilon_{ij,,}$ is calculated between two atoms *i* and *j*. $\upsilon_{ij}$ is the summation of the bond valences of individual bonds, which should sum up to the expected valence of the central atom. $R_{ij}$ is a unitless parameter characteristic of the atom pair forming the bond and $d_{ij}$ is the experimental bond length. Bond valence parameters $R_{ij}$ for calculations in this study were obtained from Brown and Altermatt[19] or Brese and O'Keeffe[20]. The universal constant, b, is reported as 0.37.[19, 20]

# CHAPTER 4

# EXPERIMENTAL RESULTS AND DISCUSSION

The main purpose of this project was to synthesize and characterize $Ca_2Mn_2N_xO_yF_z$ (with x + y + z = 5 or 6) phases to explore their potential CMR behavior. The specific compositions targeted in this study were $Ca_2Mn_2O_4N$ and $Ca_2Mn_2O_5F$.

## Synthesis of $Ca_2Mn_2O_4N$, Scheme 1

There were several attempts to directly synthesize $Ca_2Mn_2O_4N$ through standard ceramic methods. The first proposed reaction scheme is listed in **Equation 4.1**.

$$2\ CaCO_3 + MnO_2 + Mn\ (s) + \tfrac{1}{2}\ N_2 \rightarrow Ca_2Mn_2O_4N + 2\ CO_2 \qquad \textbf{Eq. 4.1}$$

### Synthesis Trial 1

In the first synthesis trial, 0.713 g of (0.00707 mol) $CaCO_3$, 0.304 g (0.00350 mol) $MnO_2$, and 0.193 g Mn (0.00351 mol) were used. The heating and cooling rates are given in **Table 4.1**. The reaction took approximately 133 hours to complete.

**Table 4.1** Furnace Program for the Attempted Synthesis of $Ca_2Mn_2O_4N$

| | |
|---|---|
| R1: Step | R3: 15°C/hr |
| L1 :28°C | L3: 200°C |
| D1: 0.0 hr | D3: 0.0hr |
| R2: 60°C/hr | R4: Step |
| L2: 900°C | L4: 28°C |
| D2: 72 hr | D4: End<br>D5: End |

Results indicated a mix of green crystals, which was verified by single crystal X-ray diffraction to be MnO. Excess white powder was also present, which was most likely unreacted CaO.

Synthesis Trial 2

For Trial 2, 0.292 g (0.00336 mol) $MnO_2$, 0.695 g (0.00689 mol) $CaCO_3$, and 0.186 g (0.00339 mol) Mn were used. The reactants were held at 900°C for only 12 hours instead of 72 hours and cooled at a slightly lower rate than in Trial 1.

**Table 4.2** Furnace Program for the Attempted Synthesis of $Ca_2Mn_2O_4N$

| | |
|---|---|
| R1: Step | R3: 10°C/hr |
| L1: 28°C | L3: 200°C |
| D1: 0.0 hr | D3: 0.0 hr |
| R2: 60°C/hr | R4: Step |
| L2: 900°C | L4: 28°C |
| D2: 12hr | D4: End<br>D5: End |

The final product again contained green MnO crystals, with white CaO powder also present. Several reddish-brown colored samples were also observed that appeared to be well formed single crystals with rectangular prism like shapes. However, X-ray diffraction analysis indicated that these crystals were actually powder samples. It appeared that a single crystalline phase was initially formed at a certain temperature, but a phase change occurred upon cooling such that the crystal shape was retained but not the crystal structure.

Synthesis Trial 3

In the first two trials, the compound appeared to undergo a phase change during the cooling process. For Trial 3, the quenching, or rapid cooling method was used in order to prevent the phase change while retaining single crystallinity. After reaching the target temperature of 1000°C, the reaction was cooled to 700°C, and then stepped to room temperature. The product contained some white powder and a few fine, violet crystals. Masses of 0.309 g $MnO_2$, 0.678g $CaCO_3$, and 0.206 g Mn were used in this trial.

**Table 4.3** Furnace Program for the Attempted Synthesis of $Ca_2Mn_2O_4N$

| | |
|---|---|
| R1: Step | R3: 10 °C/hr |
| L1: 28°C | L3: 700°C |
| D1: 0.0 hr | D3: 0.0hr |
| R2: 60°C/hr | R4: Step |
| L2: 1000°C | L4: 28°C |
| D2: 12 hr | D4: End<br>D5: End |

This reaction produced mostly green and white powder with some purple crystals. Three crystals were analyzed. The first two samples appeared to be single crystalline but did not diffract well. The third sample diffracted better but not enough data could be collected to obtain a unit cell.

Synthesis Trial 4

The quenching method used in Trial 3 seemed to be the most promising reaction approach at this point. The exact temperature at which the phase change took place was unclear. The reaction for this trial was quenched to 900°C instead of 700°C.

**Table 4.4** Furnace Program for the Attempted Synthesis of $Ca_2Mn_2O_4N$

| | |
|---|---|
| R1: Step | R3: Step |
| L1: 28°C | L3 : 900°C |
| D1: 0.0 hr | D3: 0.0hr |
| R2: 60°C/hr | R4: Step |
| L2: 1000 °C | L4: 28 °C |
| D2: 12hr | D4: End<br>D5: End |

MnO and CaO were again found in the product mixture. Several crystals were isolated but not enough data could be collected to solve the structure.

Synthesis Trial 5

For this trial, 0.461 g Mn, 1.704 g $CaCO_3$, and 0.679 g $MnO_2$ were used. The reactants were slowly cooled to 800°C instead of 700°C.

**Table 4.5** Furnace Program for the Attempted Synthesis of $Ca_2Mn_2O_4N$

| | |
|---|---|
| R1: Step | R3: 10°C/hr |
| L1: 28°C | L3: 800°C |
| D1: 0.0 hr | D3: 0.0hr |
| R2: 60°C/hr | R4: Step |
| L2: 1100°C | L4: 28°C |
| D2: 12hr | D4: End |
| | D5: End |

The product contained black crystals and white powder. Single crystal X-ray diffraction analysis indicated the black crystal was $MnO_2$.

Synthesis Trial 6

For Trial 6, 0.241 g $CaCO_3$, 0.066 g Mn, and 0.107 g $MnO_2$ were used. In an attempt to reproduce the finely shaped crystals found after Trial 1, the same reaction conditions in **Table 4.1** were used. This resulted in more MnO and CaO.

**Synthesis of $Ca_2Mn_2O_4N$, Scheme 2**

After several unsuccessful attempts to prepare $Ca_2Mn_2O_4N$ using Mn metal and $MnO_2$, a new reaction scheme was proposed using Ca metal and $Mn_2O_3$. $Mn_2O_3$ was chosen along with Ca since they should be relatively easier to oxidize.

$$Ca\ (s) + CaCO_3 + Mn_2O_3 + ½\ N_2 \rightarrow Ca_2Mn_2O_4N + CO_2 \qquad \textbf{Eq. 4.2}$$

Trial 1

For the first trial, 0.184 g (0.00118 mol) $Mn_2O_3$ and 0.154 g (0.00153 mol) Mn were used.

**Table 4.6** Furnace Program for the Attempted Synthesis of $Ca_2Mn_2O_4N$

| | |
|---|---|
| R1: Step | R3: 10°C/hr |
| L1: 28°C | L3: 700°C |
| D1: 0.0 hr | D3: 0.0 hr |
| R2: 60°C/hr | R4: Step |
| L2: 1100°C | L4: 28°C |
| D2: 12hr | D4: End<br>D5: End |

This reaction resulted in green and orange crystals. The green material is probably MnO, as often observed in previous reaction trials. The orange crystals were amorphous. Interestingly, Strozewski[21] also found orange crystals in his attempted preparations of both $BaMnNF_2$ and $SrMnNF_2$, which single X-ray analysis showed to be powder-like for the Ba sample (and so yielded no unit cell data), and amorphous for the Sr case. These observations suggest that the orange material is likely a Mn phase of some type.

Trial 2

For the second trial, 0.432 g (0.00277 mol) $Mn_2O_3$ and 0.711 g (0.00705 mol) $CaCO_3$ were used under the same conditions given in **Table 4.6** for the first synthesis trial. More green crystals were found. X-ray diffraction data indicated MnO. Evidently, $Mn_2O_3$ disproportionates to $MnO_2$ and MnO under these reaction conditions.

**Synthesis of $Ca_2Mn_2O_5F$**

As the direct synthesis of Ca-Mn-O-N compounds has yielded little success, the formation of N-O bonds in this system appears to be thermodynamically unfavorable under these reaction conditions. Therefore, other synthetic routes are currently being investigated for future work that achieve a $Mn^{3+/4+}$ mixed oxidation state in $CaMnO_3$ through anion substitution. The most promising route appears to be the reduction of $CaMnO_3$ followed by the fluorination of the product to eventually yield $Ca_2Mn_2O_5F$.

Since $CaMnO_3$ is not available commercially, the first step would be to synthesize the compound by following **Equation 4.3**, as given by Zhou *et al.*[22]

$$MnO_2 + CaCO_3 \rightarrow CaMnO_3 + CO_2 \qquad \textbf{Eq. 4.3}$$

Attempts to prepare $CaMnO_3$ via this route were unsuccessful.

An alternative route to obtaining $CaMnO_3$ is the sol gel process. The sol gel technique is a condensation reaction that forms fine particles of uniform size. The reaction generally begins with a metal alkoxide, which is produced when a metal reacts with an alcohol. Water is added to react with the alkoxide and regenerate the alcohol. There are several hydroxyl groups bound to the central metal ion (Mn, in this case), creating a three-dimensional network. The gel formed is a suspension of small particles

with a gelatin consistency. The gel is heated carefully to remove all of the liquid, and the gel then becomes a finely divided metal oxide powder.[23] Monesi *et al.*[24] have successfully synthesized $CaMnO_3$ using the sol gel method in **Equation 4.4**.

$$Ca(NO_3)_2 + MnCO_3 \rightarrow CaMnO_3 \qquad \textbf{Eq. 4.4}$$

One attempt was made in this study to synthesize $CaMnO_3$ using the sol gel method, which has yielded the most promising results thus far. The reaction resulted in a navy blue powder. Powder X-ray diffraction indicated the product to be $CaMn_7O_{12}$, which is a rhombohedral phase with a diffraction pattern very similar to that of the orthorhombic $CaMnO_3$ target, as indicated in **Figure 4.1**.

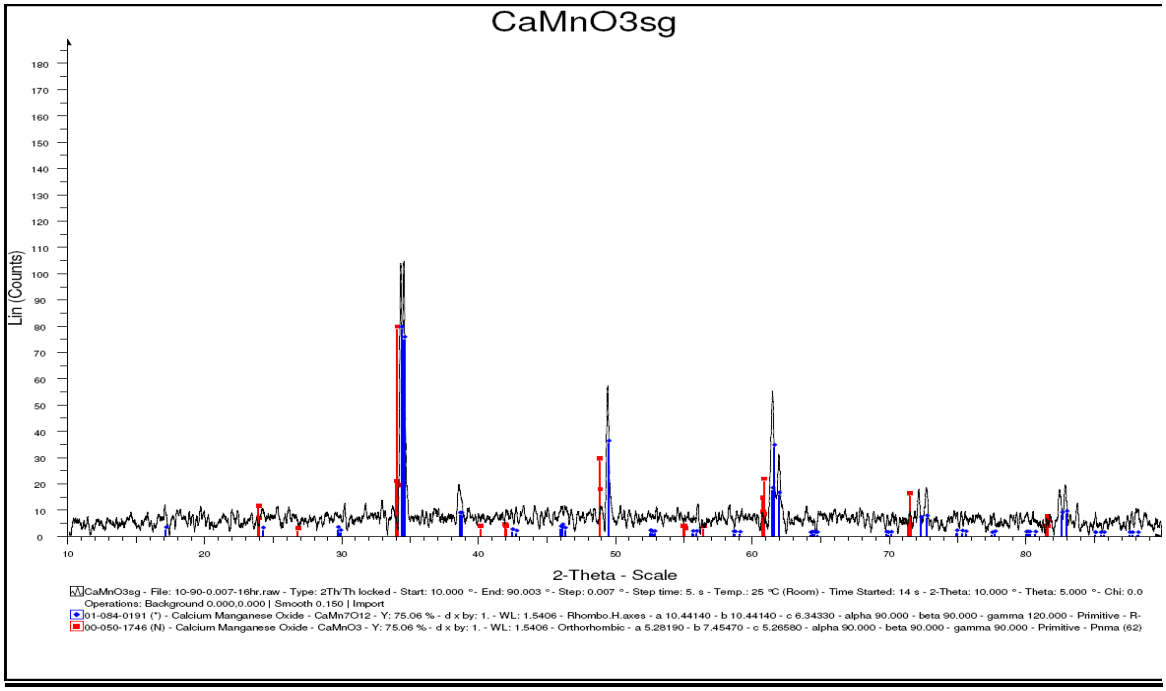


**Figure 4.1** X-ray powder diffraction pattern of the product from the sol gel synthesis of $CaMnO_3$. The experimental peaks best match the database pattern for $CaMn_7O_{12}$ (blue lines), which is very close to the expected pattern for $CaMnO_3$ (red lines).

Once successfully synthesized, $CaMnO_3$ could then be reduced to $Ca_2Mn_2O_5$ by the following reaction:

$$2\ CaMnO_3 + 2/3\ NH_3 \rightarrow Ca_2Mn_2O_5 + H_2O + 1/3\ N_2 \qquad \textbf{Eq. 4.5}$$

Poeppelmeier *et al*.[25] successfully completed the reaction listed in **Equation 4.5**. This reaction is done at a low temperature (300-325°C) to prevent the formation of the rock salt phase, $CaMnO_2$. Due to the low temperature used in the reaction, a long duration of time (over 100 hr) is usually needed to successfully prepare $CaMnO_{2.5}$ from $CaMnO_3$.

The product of this reaction will be fluorinated in the following reaction:

$$Ca_2Mn_2O_5 + NH_4HF_2 \rightarrow 2\ CaMnO_2F + NH_3 + H_2O \qquad \textbf{Eq. 4.6}$$

Finally, the fluorinated product will be combined with $CaMnO_3$ to obtain the final product, $Ca_2Mn_2O_5F$.

$$CaMnO_2F + CaMnO_3 \rightarrow Ca_2Mn_2O_5F \qquad \textbf{Eq. 4.7}$$

## Conclusions

The primary focus of this thesis was the synthesis and characterization of the novel mixed anion manganites, $Ca_2Mn_2O_4N$ and $Ca_2Mn_2NO_5F$. Unfortunately, the syntheses trials of these compounds have thus far been unsuccessful, usually resulting in preferential formation of simpler compounds such as MnO. As a result of this research, it is concluded that the direct synthesis of such compounds through direct ceramic methods is not favorable, and therefore other routes must be investigated. In particular, it can be

concluded that oxidation of Mn metal is not an energetically feasible pathway for the synthesis of oxynitrides, as observed previously by Strozewski[21] in work involving M-Mn-N-F (M = Sr, Ba) systems. The most promising route for the preparation of the target oxyfluoride compound appears to be the proposed reduction and subsequent fluorination of $CaMnO_3$, which will be the focus of future work.

# CHAPTER 5

## SINGLE CRYSTAL X-RAY DIFFRACTION RESULTS FOR $Sr_2BiGa_{11}O_{20}$

This chapter is focused on the first single crystal X-ray diffraction study of $Sr_2BiGa_{11}O_{20}$.

### Background

$Sr_2BiGa_{11}O_{20}$ appears to be isostructural to $Ba_2BiGa_{11}O_{20}$, a compound also made by the Wagner group at YSU.[26] Haberey *et al.*[27] previously reported discovering this phase during the preparation of $SrGa_{12}O_{19}$ crystals from a $Bi_2O_3$ flux. However, the structure for the $Sr_2BiGa_{11}O_{20}$ phase has not been reported. These $A_2BC_{11}O_{20}$ phases are closely related to a series of $A_3BC_{10}O_{20}$ phases (with A = Sr, Ba, & Pb; B = Si, Ge, Sn, & Ti; and C = Al, Ga, & Fe), all of which are monoclinic with cell parameters very similar to those of our phases.[28-30] The ideal structure for the $A_3BC_{11}O_{20}$ compounds is shown in **Figure 5.1** As indicated in the figure, the major structural feature of these compounds is the tetrahedral framework made up of layers of tetrahedra of C-type atoms two units wide, with the layers "stacked" along the *a* axis. The successive layers are related by the twofold symmetry along the *b* axis, and are linked together by corner-sharing to a chain of octahedra of C-type atoms running parallel to the c-axis. There are two types of A atom sites, as shown in Figure 5.1. A(1) atoms are octahedrally coordinated, and A(2) atoms have a coordination of 7, 8, or 9, depending on composition.[28-30] B-type atoms share the two octahedrally coordinated C-type sites, viz. C(1) and C(2), which are 2b and 4h sites, respectively. As further discussed below, the structure of our $A_2BiGa_{11}O_{20}$ phases differ only in that B-type atoms (i.e. Bi for our case) share the A(2)-type site rather than the C-type sites as in $A_3BC_{10}O_{20}$.

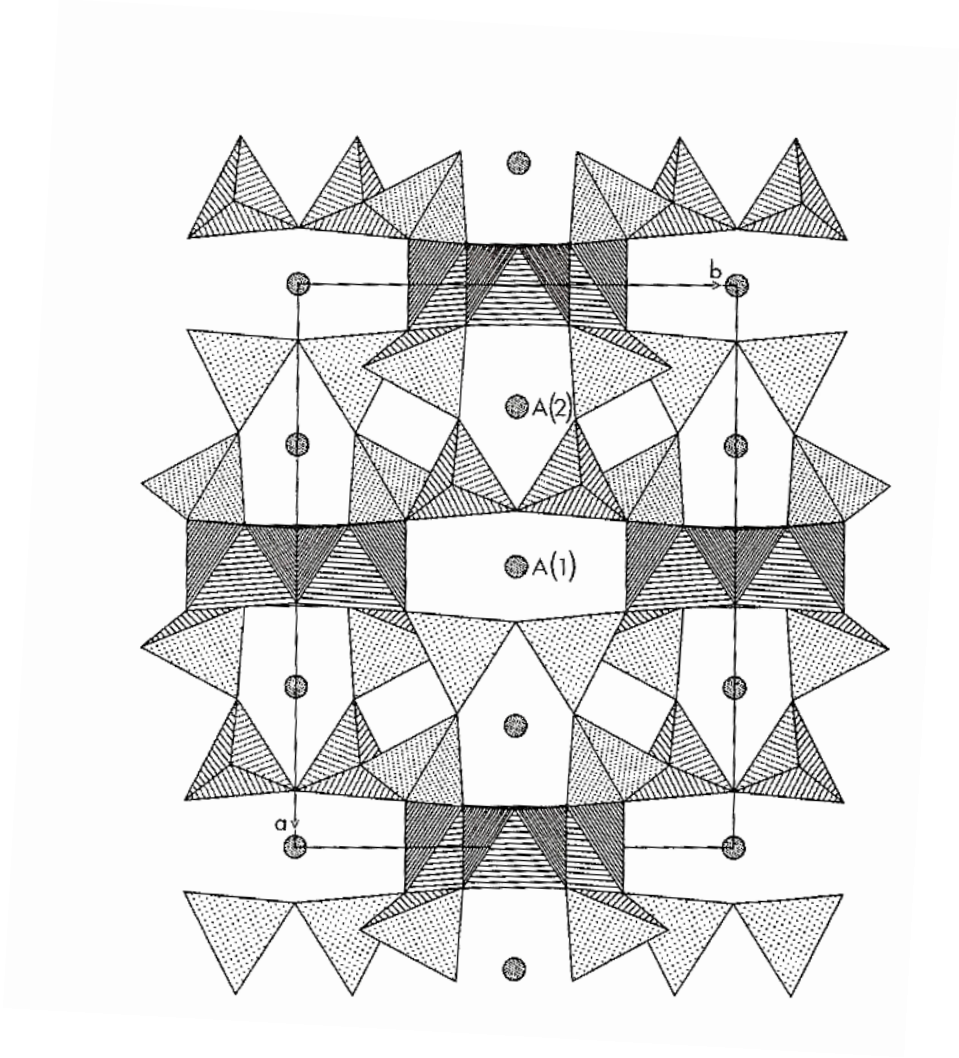


**Figure 5.1** Projection of the $A_3BC_{10}O_{20}$-type structure along [001][26]

**Experimental**

Following a protocol given by Haberey *et al.*[27], samples from the SrO-$Ga_2O_3$ system were synthesized using a $Bi_2O_3$ flux, creating hexagonal crystals of $SrGa_{12}O_{19}$ and monoclinic crystals of $Sr_2BiGa_{11}O_{20}$. A 20/50/30% mol% mixture of $SrCO_3/Ga_2O_3/Bi_2O_3$ was heated in air in a covered Pt crucible at a rate of 60°C/hr to 1350°C, and held for 5 hours. The mixture was then cooled to 500°C at a rate of 20°C/hr, and then to room temperature at a rate of 50°C/h. A suitable crystal of the $Sr_2BiGa_{11}O_{20}$ phase was selected for X-ray single crystal analysis, and data was collected on site using a Bruker SMART APEX CCD system. Structure solution and refinement was performed via the SHELXTL software package, version 6.14.

**Structure Description**

The unit cell parameters obtained for $Sr_2BiGa_{11}O_{20}$ are: a = 14.548 Å, b = 11.6842 Å, c = 5.1032 Å, and β = 90.855. For $Ba_2BiGa_{11}O_{20}$, the cell parameters are: a = 14.9283 Å, b = 11.7046 Å, c = 5.1170 Å, and β = 91.137.[26] Comparison of these parameters strongly suggests that the compounds are isostructural, and this was verified by the structure refinement analysis. Although the standard choice of space group for this system is C2/m (No. 12), the I2/m setting was chosen here to be consistent with previously published structures of related compounds.[26, 28-30] A complete summary of the crystal data and refinement results for $Sr_2BiGa_{11}O_{20}$ is shown in Table 1 of the Appendix. A structure plot for the compound projected along [001] is shown in **Figure 5.2**. Atomic positions and equivalent isotropic displacement parameters are given in Table 2 of the Appendix, and distances and bond angles are given in Table 3.

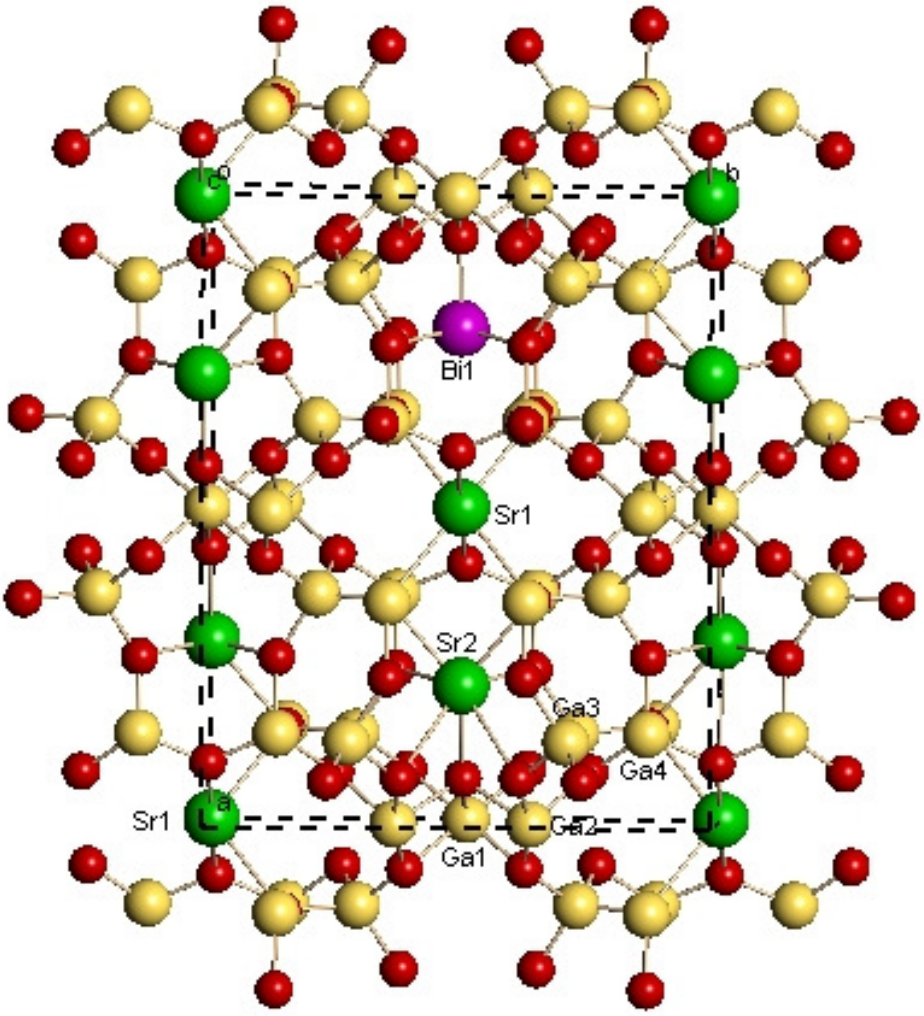


**Figure 5.2** Structure plot for $Sr_2BiGa_{11}O_{20}$ projected along [001]. Green spheres are Sr, violet spheres are Bi, yellow spheres are Ga, and red spheres are O atoms. Bi and Sr(2) share a position that is 50% occupied by each atom; Bi is shown in only one site.

An important feature of the $M_2BiGa_{11}O_{20}$ (M = Sr, Ba) structure is the relative positioning of the M and Bi atoms. As mentioned for the present case, Sr(2) and Bi atoms essentially share a site, although the positions are actually shifted by 0.427 Å along the c-direction. The reason for the slight displacement of the positions relative to one another is most likely due to the stereochemically active $6s^2$ lone pair on the Bi atom. While a stereochemically active lone pair basically behaves as a ligand, the lone pair – nucleus attraction is stronger in general than a bonding pair – nucleus attraction,[26] and it is this effect that causes the Bi atom to shift away from the polyhedral center. **Figure 5.3** shows the local coordination environment for the Bi(1) and Sr(2) atoms. It can be seen from the figure that for the Sr(2) site, the atom is coordinated to all seven oxygen atoms shown, whereas the Bi atom has shifted off position and is coordinated to only its three nearest oxygen atoms. (Note that the Bi-O(3) and Bi-O(5) distances are 2.835 and 3.094 Å, respectively, which is too long for Bi-O bonds, cf. Bi-O(6), which is 2.249 Å). The displacement of the Bi atom suggests that its stereochemically active lone pair is directed towards the Sr(2) position, acting as a fourth unseen ligand for Bi.

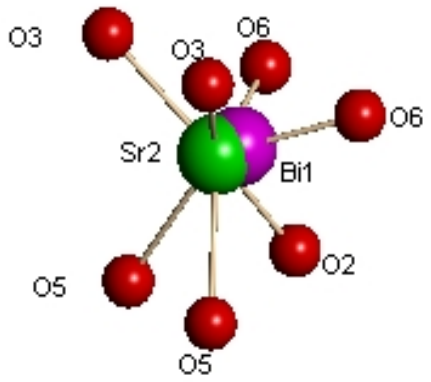


**Figure 5.3** Local coordination environment showing the relative positions of the Sr(2) and Bi sites, which are 0.427 Å apart.

A localized ORTEP-type plot (75% ellipsoids) for the Sr(1) and Sr(2)/Bi(1) sites projected along [001] is given in **Figure 5.4**. The figure shows that the displacement of many of the atoms tends to be largest towards the Sr(2)/Bi(1) site, particularly for O(1), O(3) and O(6). This is not surprising since the average oxygen positions would be expected to change slightly depending upon whether Sr(2) or Bi(1) is present at a particular local site.

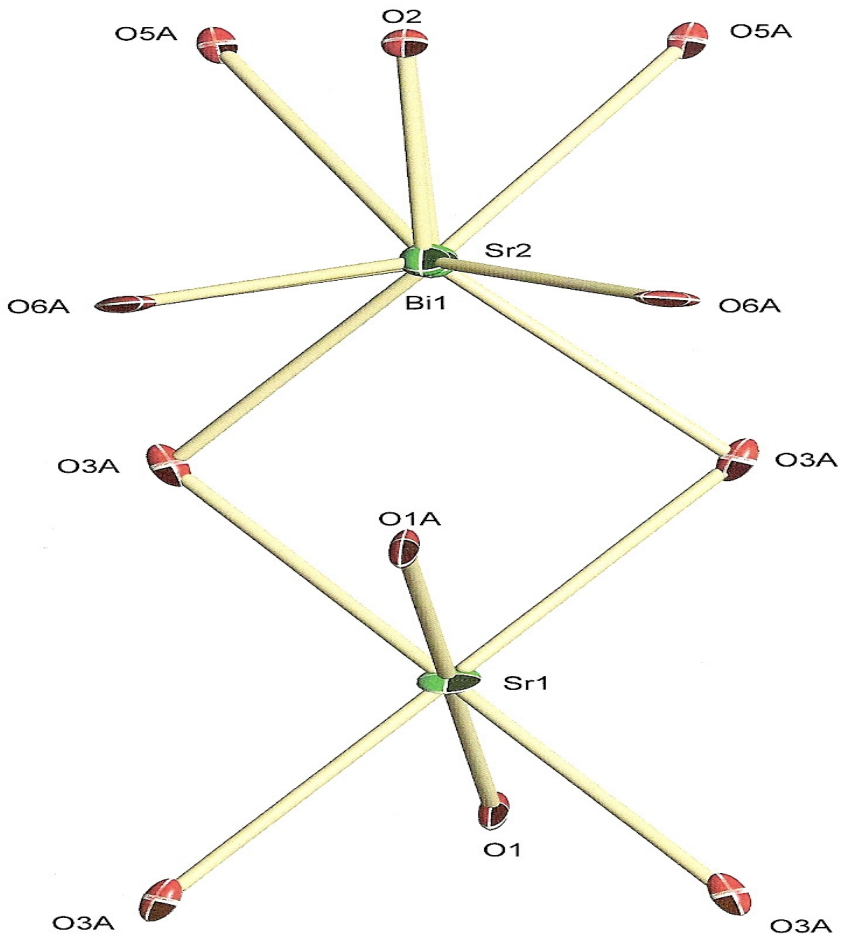


**Figure 5.4** Localized ORTEP-type plot (75% ellipsoids) for the Sr(1) and Sr(1)/Bi(1) sites projected along the [001] direction.

**Bond Valence Analysis**

Individual bond valence calculations were made using **Equation 3.1**. The bond valence parameters used were those reported by Brown and Altermatt,[19] since these were the values used for the previous study of $Ba_2BiGa_{11}O_{20}$.[26] The values are $R_{ij}$ = 2.118, 2.094, and 1.730 for Sr-O, Bi-O, and Ga-O bonds, respectively. The results are listed in **Table 5.1**. Each of the four gallium positions and most of the oxygen sites have bond valence sums very close to the expected values (i.e. the oxidation numbers). The largest deviations in the table are for Sr(1) and Bi(1) which are quite underbonded. The Bi(1) sum of 2.031 is much lower than the expected value of 3.0, although this is not surprising considering that the $6s^2$ lone pair "ligand" is not taken into account in the calculations. Sr(1) is also severely underbonded, in part because of elongation of Sr(1)-O(3) bonds due to the influence of the adjacent Sr(2)/Bi(1) site. As indicated in **Figure 5.4** above, the O(3) atoms bridge the Sr(1) and Sr(2)/Bi(1) sites. When Bi is present at the latter site, the stronger attraction of the $6s^2$ lone pair pulls the O(3) atoms relatively closer to itself and away from the Sr(1) atom, weakening the bonding of the site on average. Thus for Sr(1)-O(3), the bond distance is 2.749 Å while it is 2.678 Å for the Sr(2)-O(3) bonds.

Also of interest in **Table 5.1** is the comparison of bond valences for the Sr phase obtained here to those of the Ba phase (shown in parentheses in the table) obtained previously.[26] In particular, note that Sr(2) is underbonded (i.e. 1.772) in our case, while in the Ba phase, Ba(2) is overbonded (i.e. 2.245). Also, Sr(1) in the present phase is relatively more underbonded than Ba(1) in the Ba phase, i.e. the bond valence values are 1.482 vs. 1.626, respectively. The explanation for both trends is likely related to the fact that although the Sr lattice is smaller than the Ba lattice (867 vs. 894 $Å^3$, respectively),

the decrease is not as significant as would be expected if it were driven solely by the substitution of Sr for Ba. For example, the volume of BaO rocksalt is 170 $Å^3$, and this decreases to 138 $Å^3$ for SrO (note that the MO and $M_2BiGa_{11}O_{20}$ lattices both contain four M cations). For the present case, lattice size is driven largely by the Ga-O framework, as indicated by the presence of nearly ideal bond valence sums for Ga atoms in both the Sr and Ba phases according to **Table 5.1**. Thus, the M sites are somewhat more relaxed than optimal for Sr-O bonds in the lattice relative to the case for Ba-O bonds, accounting for the observed trends for Sr vs. Ba bond valence sums. On the other hand, the somewhat smaller Sr lattice apparently allows for Bi-O bonds that are shortened enough to account for the fact that Bi appears less underbonded in the Sr case (2.031) than in the case of the Ba phase (1.771).

**Table 5.1** Bond Valence Sums ($V_{ij}$) For $Sr_2BiGa_{11}O_{20}$

| | $\upsilon_{ij}=\upsilon_{ji}$ **Anions** | | | | | | |
|---|---|---|---|---|---|---|---|
| **Cations** | O(1) | O(2) | O(3) | O(4) | O(5) | O(6) | ***$V_{ij}=\sum\upsilon_{ij}$ for Cations (→)** |
| Sr(1) | 0.377 (× 2) → (× 1)↓ | | 0.182 (× 4) → (× 1)↓ | | | | **1.482** *(1.626)* |
| Sr(2) | | 0.470 (× 1) → (× 1)↓ | 0.220 (× 2) → (× 1)↓ | | 0.128 (× 2)→ (× 1)↓ | 0.303 (× 2) → (× 1)↓ | **1.772** *(2.245)* |
| Bi(1) | | 0.715 (× 1) → (× 1)↓ | | | | 0.658 (× 2) → (× 1)↓ | **2.031** *(1.771)* |
| Ga(1) | | 0.564 (× 2) → (× 1)↓ | | | 0.468 (× 4) → (× 1)↓ | | **3.000** *(2.984)* |
| Ga (2) | | 0.415 (× 2) → (× 2)↓ | | 0.546 (× 2) → (× 1)↓ | 0.565 (× 2) → (× 1)↓ | | **3.052** *(2.990)* |
| Ga(3) | | | 0.731 (× 1) → (× 1)↓ | 0.713 (× 1) → (× 1)↓ | 0.776 (× 1) → (× 1)↓ | 0.737 (× 1) → (× 1)↓ | **2.957** *(3.003)* |
| Ga(4) | 0.786 (× 1) → (× 2)↓ | | 0.755 (× 1) → (× 1)↓ | 0.739 (× 1) → (× 1)↓ | | 0.745 (× 1) → (× 1)↓ | **3.025** *(2.976)* |
| ***$V_{ij}=\sum\upsilon_{ij}$ for Anions (↓)** | **1.949** *(1.955)* | **with Sr(2) 1.864** *(1.905)* **with Bi(1) 2.109** *(2.013)* | **1.888** *(2.039)* | **1.998** *(1.932)* | **1.937** *(2.010)* | **with Sr(2) 1.785** *(1.839)* **with Bi(1) 2.140** *(2.040)* | |

* Bond valence sums in parentheses are values for $Ba_2BiGa_{11}O_{20}$ from ref. 26, for comparison.

## REFERENCES


1. Di Salvo, F.J., *Solid State Communications*, **102**, 79-85, (1997).
2. West, A. R. Basic Solid State Chemistry, John Wiley and Sons: New York; 1988
3. Glusker, J.P.; Lewis, M.; Rossi, M., *Crystal Structure Analysis for Chemists and Biologists.* VCH: New York; 1994.
4. http://serc.carleton.edu/research_education/geochemsheets/BraggsLaw.html
5. http://en.wikipedia.org/wiki/Perovskite
6. von Helmolt, R., Wecker, J., Holzapfel, B., Schultz, L., and Samwer, K., *Phys. Rev. Lett.,* **71**, 2331-2333 (1993).
7. Ramirez, A.P., *J. Phys: Condens. Mater*., **9**, 8171-8194 (1997).
8. Zeng, Z., Greenblatt, M. and Croft, M., *Phys. Rev. B*, **54**, 8784-8788, (1999).
9. Preuss, P. www.lbl.giv/Science-Articles/Archive/colossal-magnetoresistance.html, July 5, 2001.
10. http://en..wikipedia.org/wiki/Double-exchange mechanism
11. www-attfield.ch.cam.ac.uk/MOP.html
12. Volkova, O., Goodilin, E., Vasiliev, A., Tristan, N., Kerschl, P., Skourski, Y., Mueller, K.H., Buechner, B., *JETP Letters,* **82(10)**, 642-645 (2005).
13. Schmid, S. and Withers, R.L., *J. of Solid St. Chem.,* **109**, 391-400 (1994).
14. Vogt, T. and Schweda, E., *J. of Solid St. Chem.,* **100(2)**, 246-54 (1992).
15. Abrait, N., Laval, J.P., Frit, B., and Roult, G., *Acta Cryst. B*, 38, 1088-1093 (1982).
16. Jack, D.J., M.S. Thesis, Youngstown State University, Youngstown, OH, Aug. 2007.
17. Reyes-Garcia, E.A., Sun, Y., Reyes-Gil, K., and Raftery, D., *J. Phys. Chem.* **111**, 17146-17154 (2007).

18. Kim, Y.I., Woodward, P.M., Baba-Kishi, K.Z., and Tai, C.W., *Chem. Mater*., **16**, 1267-1276 (2004).

19. Brown, I.D. and Altermatt, D., *Acta Crystallgr*., **B 41**, 244 (1985).

20. Brese, N.E. and O'Keeffe, M., *Acta Crystallgr*., **B 47,** 192 (1991).

21. Strozewski, M.S., M.S. Thesis, Youngstown State University, Youngstown, OH, August 2007.

22. Zhou, Q. and Kennedy, B., *J. of Physics and Chemistry of Solids.,* **67**, 1595-1598 (2006).

23. Brown, T; LeMay, H., Bursten, B. and Burdge, J., *Chemistry: The Central Science,* 9th ed., Prentice Hall: New Jersey; 2003.

24. Monesi, C. Meneghini, C., Bardelli, F., Benfatto, M., Mobilio, S., Manju, U., and Sarma, D.D., *Physical Rev. B*, **72,** 174104, (2005).

25. Poeppelmeier, K.R., Leonowicz, M.E., and Longo, J.M., *J. of Solid State Chem.,* **44,** 89-98 (2004).

26. Wagner, T.R. and Styranec, T.J., *Journal of Solid St. Chem.,* **313-320,** (1998).

27. Haberey, F., Leckebusch, R., Rosenberg, M., and Sahl, K., *J. Cryst. Growth* **61,** 284 (1983).

28. Vinek, H., Völlenkle, H., and Nowotny, H., *Monatsh. Chem.*, **101**, 275 (1970).

29. Cadée, M.C., Ijdo, D.J.W., and Blasse, G., *J. Solid State Chem*., **41**, 39 (1982).

30. Cadée, M.C., Verschoor, G.C., and IJdo, D.J.W., *Acta Crystallogr.,* **C 39**, 921 (1983).

# APPENDIX

## CRYSTALLOGRAPHY DATA FOR $Sr_2BiGa_{11}O_{20}$

**Table 1**. Crystal data and structure refinement for $Sr_2$ Bi $Ga_{11}$ $O_{20}$.

| | |
|---|---|
| Empirical formula | $Sr_2$ Bi $Ga_{11}$ $O_{20}$ |
| Formula weight | 1471.14 |
| Crystal size (nm) | 0.13 x 0.07 x 0.05 mm |
| Crystal color | Light yellow |
| Space Group | I2/m |
| a (Å) | 14.548(2) |
| b (Å) | 11.6842(15) |
| c (Å) | 5.1032(6) |
| α | 90 |
| β | 90.855(2) |
| γ | 90 |
| V ($Å^3$) | 867.35 |
| Z | 4 |
| P calc | 5.633 $Mg/m^3$ |
| λ | 0.71073 A |
| θ range for data collection | 2.24 to 31.96 |
| Limiting indices | -21<=h<=21, -17<=k<=17, -7<=l<=7 |
| No. of Reflections Collected | 5222 |
| No. of Independent Reflections | 1488 R(int) = 0.0335] |
| Final R indices [I>2σ(I)] | R1 = 0.0375, wR2 = 0.0797 |
| Final R indices (all data) | R1 = 0.0422, wR2 = 0.0841 |
| Refinement method | Full-matrix least-squares on F^2 |
| Goodness-of-fit on F^2 | 1.121 |
| Extinction coefficient | 0.00235(14) |
| Largest diff. peak and hole | 3.480 and -4.229 e.$Å^{-3}$ |

**Table 2.** Atomic coordinates and equivalent isotropic displacement parameters ($Å^2$ x $10^3$) for $Sr_2$ Bi $Ga_{11}$ $O_{20}$. U(eq) is defined as one third of the trace of the orthogonalized $U_{ij}$ tensor.

| Atom | Site | x | y | z | U(eq) |
|---|---|---|---|---|---|
| Sr(1) | 2a | 0 | 0 | 0 | 14(1) |
| Sr(2) | 4i | 0.7183(3) | 0 | 0.9858(5) | 14(1) |
| Bi(1) | 4i | 0.7159(1) | 0 | 0.10691(2) | 14(1) |
| Ga(1) | 2b | 0.5000 | 0 | 0.5000 | 6(1) |
| Ga(2) | 4h | 0.5000 | 0.1336(1) | 0 | 3(1) |
| Ga(3) | 8j | 0.1367(1) | 0.7157(1) | 0.9786(1) | 4(1) |
| Ga(4) | 8j | 0.1423(1) | 0.8641(1) | 0.4930(1) | 4(1) |
| O(1) | 4i | 0.0948(5) | 0 | 0.6002(16) | 15(1) |
| O(2) | 4i | 0.5687(5) | 0 | 0.1767(12) | 7(1) |
| O(3) | 8j | 0.1440(3) | 0.8582(4) | 0.1340(9) | 10(1) |
| O(4) | 8j | 0.0790(3) | 0.7500(4) | 0.6616(8) | 6(1) |
| O(5) | 8j | 0.0762(3) | 0.6173(4) | 0.1932(8) | 8(1) |
| O(6) | 8j | 0.2610(3) | 0.8651(5) | 0.6224(11) | 14(1) |

**Table 3**. Bond lengths [Å] and angles [deg] for $Sr_2BiGa_{11}O_{20}$

| | |
|---|---|
| Sr(1)-O(1)#1 | 2.479(7) |
| Sr(1)-O(1) | 2.479(7) |
| Sr(1)-O(3)#2 | 2.749(5) |
| Sr(1)-O(3)#3 | 2.749(5) |
| Sr(1)-O(3)#4 | 2.749(5) |
| Sr(1)-O(3)#5 | 2.749(5) |
| Sr(1)-Ga(4)#2 | 3.6028(7) |
| Sr(1)-Ga(4)#4 | 3.6028(7) |
| Sr(1)-Ga(4)#3 | 3.6028(7) |
| Sr(1)-Ga(4)#5 | 3.6028(7) |
| Sr(1)-Ga(4) | 3.6962(7) |
| Sr(1)-Ga(4)#6 | 3.6962(7) |
| Sr(2)-O(2) | 2.397(7) |
| Sr(2)-O(6)#6 | 2.560(6) |
| Sr(2)-O(6)#1 | 2.560(6) |
| Sr(2)-O(3)#3 | 2.678(6) |
| Sr(2)-O(3)#5 | 2.678(6) |
| Sr(2)-O(5)#7 | 2.879(6) |
| Sr(2)-O(5)#8 | 2.879(6) |
| Sr(2)-Ga(2)#9 | 3.540(3) |
| Sr(2)-Ga(2)#10 | 3.540(3) |
| Sr(2)-Ga(4)#3 | 3.571(3) |
| Sr(2)-Ga(4)#5 | 3.571(3) |
| Sr(2)-Ga(4)#6 | 3.681(3) |
| Bi(1)-O(2) | 2.218(7) |
| Bi(1)-O(6)#6 | 2.249(5) |
| Bi(1)-O(6)#1 | 2.249(5) |
| Ga(1)-O(2)#9 | 1.942(6) |
| Ga(1)-O(2) | 1.942(6) |
| Ga(1)-O(5)#11 | 2.011(5) |
| Ga(1)-O(5)#12 | 2.011(5) |
| Ga(1)-O(5)#13 | 2.011(5) |
| Ga(1)-O(5)#14 | 2.011(5) |
| Ga(1)-Ga(2)#15 | 2.9913(6) |
| Ga(1)-Ga(2) | 2.9913(6) |
| Ga(1)-Ga(2)#9 | 2.9913(6) |
| Ga(1)-Ga(2)#10 | 2.9913(6) |
| Ga(2)-O(5)#16 | 1.941(4) |
| Ga(2)-O(5)#13 | 1.941(4) |
| Ga(2)-O(4)#17 | 1.954(4) |
| Ga(2)-O(4)#14 | 1.955(4) |
| Ga(2)-O(2)#2 | 2.055(4) |
| Ga(2)-O(2)#9 | 2.055(4) |
| Ga(2)-Ga(1)#2 | 2.9913(6) |
| Ga(2)-Sr(2)#9 | 3.540(3) |
| Ga(2)-Sr(2)#2 | 3.540(3) |
| Ga(3)-O(5) | 1.824(4) |
| Ga(3)-O(6)#18 | 1.843(5) |
| Ga(3)-O(3)#2 | 1.846(5) |
| Ga(3)-O(4) | 1.855(4) |

| | |
|---|---|
| Ga(3)-Sr(2)#19 | 3.765(2) |
| Ga(3)-Sr(2)#20 | 3.791(2) |
| Ga(4)-O(1) | 1.819(4) |
| Ga(4)-O(3) | 1.834(4) |
| Ga(4)-O(6) | 1.839(5) |
| Ga(4)-O(4) | 1.842(4) |
| Ga(4)-Sr(2)#5 | 3.571(3) |
| Ga(4)-Sr(1)#10 | 3.6028(7) |
| Ga(4)-Sr(2)#1 | 3.681(3) |
| O(1)-Ga(4)#21 | 1.819(4) |
| O(2)-Ga(2)#9 | 2.055(4) |
| O(2)-Ga(2)#10 | 2.055(4) |
| O(3)-Ga(3)#10 | 1.846(5) |
| O(3)-Sr(2)#5 | 2.678(6) |
| O(3)-Sr(1)#10 | 2.749(5) |
| O(4)-Ga(2)#22 | 1.954(4) |
| O(5)-Ga(2)#19 | 1.941(4) |
| O(5)-Ga(1)#19 | 2.011(4) |
| O(5)-Sr(2)#20 | 2.879(6) |
| O(6)-Ga(3)#18 | 1.843(5) |
| O(6)-Bi(1)#1 | 2.249(5) |
| O(6)-Sr(2)#1 | 2.560(6) |
| O(1)#1-Sr(1)-O(1) | 179.999(1) |
| O(1)#1-Sr(1)-O(3)#2 | 103.08(18) |
| O(1)-Sr(1)-O(3)#2 | 76.92(18) |
| O(1)#1-Sr(1)-O(3)#3 | 76.92(18) |
| O(1)-Sr(1)-O(3)#3 | 103.08(18) |
| O(3)#2-Sr(1)-O(3)#3 | 105.88(19) |
| O(1)#1-Sr(1)-O(3)#4 | 103.08(18) |
| O(1)-Sr(1)-O(3)#4 | 76.92(18) |
| O(3)#2-Sr(1)-O(3)#4 | 74.12(19) |
| O(3)#3-Sr(1)-O(3)#4 | 180.0 |
| O(1)#1-Sr(1)-O(3)#5 | 76.92(18) |
| O(1)-Sr(1)-O(3)#5 | 103.08(18) |
| O(3)#2-Sr(1)-O(3)#5 | 179.999(1) |
| O(3)#3-Sr(1)-O(3)#5 | 74.12(19) |
| O(3)#4-Sr(1)-O(3)#5 | 105.88(19) |
| O(1)#1-Sr(1)-Ga(4)#2 | 75.30(17) |
| O(1)-Sr(1)-Ga(4)#2 | 104.70(17) |
| O(3)#2-Sr(1)-Ga(4)#2 | 29.89(9) |
| O(3)#3-Sr(1)-Ga(4)#2 | 109.63(9) |
| O(3)#4-Sr(1)-Ga(4)#2 | 70.37(9) |
| O(3)#5-Sr(1)-Ga(4)#2 | 150.11(9) |
| O(1)#1-Sr(1)-Ga(4)#4 | 75.30(17) |
| O(1)-Sr(1)-Ga(4)#4 | 104.70(17) |
| O(3)#2-Sr(1)-Ga(4)#4 | 70.37(10) |
| O(3)#3-Sr(1)-Ga(4)#4 | 150.11(9) |
| O(3)#4-Sr(1)-Ga(4)#4 | 29.89(9) |
| O(3)#5-Sr(1)-Ga(4)#4 | 109.63(9) |
| Ga(4)#2-Sr(1)-Ga(4)#4 | 52.28(2) |
| O(1)#1-Sr(1)-Ga(4)#3 | 104.70(17) |
| O(1)-Sr(1)-Ga(4)#3 | 75.29(17) |
| O(3)#2-Sr(1)-Ga(4)#3 | 109.63(9) |

| | |
|---|---|
| O(3)#3-Sr(1)-Ga(4)#3 | 29.89(9) |
| O(3)#4-Sr(1)-Ga(4)#3 | 150.11(9) |
| O(3)#5-Sr(1)-Ga(4)#3 | 70.37(10) |
| Ga(4)#2-Sr(1)-Ga(4)#3 | 127.72(2) |
| Ga(4)#4-Sr(1)-Ga(4)#3 | 180.0 |
| O(1)#1-Sr(1)-Ga(4)#5 | 104.70(17) |
| O(1)-Sr(1)-Ga(4)#5 | 75.29(17) |
| O(3)#2-Sr(1)-Ga(4)#5 | 150.11(9) |
| O(3)#3-Sr(1)-Ga(4)#5 | 70.37(9) |
| O(3)#4-Sr(1)-Ga(4)#5 | 109.63(9) |
| O(3)#5-Sr(1)-Ga(4)#5 | 29.89(9) |
| Ga(4)#2-Sr(1)-Ga(4)#5 | 180.0 |
| Ga(4)#4-Sr(1)-Ga(4)#5 | 127.72(2) |
| Ga(4)#3-Sr(1)-Ga(4)#5 | 52.28(2) |
| O(1)#1-Sr(1)-Ga(4) | 154.19(3) |
| O(1)-Sr(1)-Ga(4) | 25.81(3) |
| O(3)#2-Sr(1)-Ga(4) | 58.84(9) |
| O(3)#3-Sr(1)-Ga(4) | 89.99(10) |
| O(3)#4-Sr(1)-Ga(4) | 90.01(10) |
| O(3)#5-Sr(1)-Ga(4) | 121.16(9) |
| Ga(4)#2-Sr(1)-Ga(4) | 88.710(17) |
| Ga(4)#4-Sr(1)-Ga(4) | 110.85(2) |
| Ga(4)#3-Sr(1)-Ga(4) | 69.15(2) |
| Ga(4)#5-Sr(1)-Ga(4) | 91.290(17) |
| O(1)#1-Sr(1)-Ga(4)#6 | 25.81(3) |
| O(1)-Sr(1)-Ga(4)#6 | 154.19(3) |
| O(3)#2-Sr(1)-Ga(4)#6 | 89.99(10) |
| O(3)#3-Sr(1)-Ga(4)#6 | 58.84(9) |
| O(3)#4-Sr(1)-Ga(4)#6 | 121.16(9) |
| O(3)#5-Sr(1)-Ga(4)#6 | 90.01(10) |
| Ga(4)#2-Sr(1)-Ga(4)#6 | 69.15(2) |
| Ga(4)#4-Sr(1)-Ga(4)#6 | 91.290(17) |
| Ga(4)#3-Sr(1)-Ga(4)#6 | 88.710(17) |
| Ga(4)#5-Sr(1)-Ga(4)#6 | 110.85(2) |
| Ga(4)-Sr(1)-Ga(4)#6 | 129.13(2) |
| O(2)-Sr(2)-O(6)#6 | 77.27(18) |
| O(2)-Sr(2)-O(6)#1 | 77.27(18) |
| O(6)#6-Sr(2)-O(6)#1 | 76.0(3) |
| O(2)-Sr(2)-O(3)#3 | 141.22(12) |
| O(6)#6-Sr(2)-O(3)#3 | 73.60(17) |
| O(6)#1-Sr(2)-O(3)#3 | 118.6(2) |
| O(2)-Sr(2)-O(3)#5 | 141.22(12) |
| O(6)#6-Sr(2)-O(3)#5 | 118.6(2) |
| O(6)#1-Sr(2)-O(3)#5 | 73.60(17) |
| O(3)#3-Sr(2)-O(3)#5 | 76.4(2) |
| O(2)-Sr(2)-O(5)#7 | 64.00(18) |
| O(6)#6-Sr(2)-O(5)#7 | 100.80(16) |
| O(6)#1-Sr(2)-O(5)#7 | 140.6(2) |
| O(3)#3-Sr(2)-O(5)#7 | 96.96(15) |
| O(3)#5-Sr(2)-O(5)#7 | 135.24(16) |
| O(2)-Sr(2)-O(5)#8 | 64.00(18) |
| O(6)#6-Sr(2)-O(5)#8 | 140.6(2) |
| O(6)#1-Sr(2)-O(5)#8 | 100.80(15) |

| | |
|---|---|
| O(3)#3-Sr(2)-O(5)#8 | 135.24(16) |
| O(3)#5-Sr(2)-O(5)#8 | 96.96(15) |
| O(5)#7-Sr(2)-O(5)#8 | 56.83(19) |
| O(2)-Sr(2)-Ga(2)#9 | 34.09(10) |
| O(6)#6-Sr(2)-Ga(2)#9 | 78.92(12) |
| O(6)#1-Sr(2)-Ga(2)#9 | 110.53(15) |
| O(3)#3-Sr(2)-Ga(2)#9 | 113.97(11) |
| O(3)#5-Sr(2)-Ga(2)#9 | 162.18(15) |
| O(5)#7-Sr(2)-Ga(2)#9 | 33.21(10) |
| O(5)#8-Sr(2)-Ga(2)#9 | 65.36(12) |
| O(2)-Sr(2)-Ga(2)#10 | 34.09(10) |
| O(6)#6-Sr(2)-Ga(2)#10 | 110.53(15) |
| O(6)#1-Sr(2)-Ga(2)#10 | 78.92(12) |
| O(3)#3-Sr(2)-Ga(2)#10 | 162.18(15) |
| O(3)#5-Sr(2)-Ga(2)#10 | 113.97(11) |
| O(5)#7-Sr(2)-Ga(2)#10 | 65.36(12) |
| O(5)#8-Sr(2)-Ga(2)#10 | 33.21(10) |
| Ga(2)#9-Sr(2)-Ga(2)#10 | 52.33(6) |
| O(2)-Sr(2)-Ga(4)#3 | 143.73(14) |
| O(6)#6-Sr(2)-Ga(4)#3 | 101.50(14) |
| O(6)#1-Sr(2)-Ga(4)#3 | 138.29(17) |
| O(3)#3-Sr(2)-Ga(4)#3 | 30.02(10) |
| O(3)#5-Sr(2)-Ga(4)#3 | 71.60(12) |
| O(5)#7-Sr(2)-Ga(4)#3 | 81.05(10) |
| O(5)#8-Sr(2)-Ga(4)#3 | 105.51(12) |
| Ga(2)#9-Sr(2)-Ga(4)#3 | 109.68(6) |
| Ga(2)#10-Sr(2)-Ga(4)#3 | 136.79(10) |
| O(2)-Sr(2)-Ga(4)#5 | 143.73(14) |
| O(6)#6-Sr(2)-Ga(4)#5 | 138.29(17) |
| O(6)#1-Sr(2)-Ga(4)#5 | 101.50(14) |
| O(3)#3-Sr(2)-Ga(4)#5 | 71.60(12) |
| O(3)#5-Sr(2)-Ga(4)#5 | 30.02(10) |
| O(5)#7-Sr(2)-Ga(4)#5 | 105.51(12) |
| O(5)#8-Sr(2)-Ga(4)#5 | 81.05(10) |
| Ga(2)#9-Sr(2)-Ga(4)#5 | 136.79(10) |
| Ga(2)#10-Sr(2)-Ga(4)#5 | 109.68(6) |
| Ga(4)#3-Sr(2)-Ga(4)#5 | 52.79(5) |
| O(2)-Sr(2)-Ga(4)#6 | 101.54(16) |
| O(6)#6-Sr(2)-Ga(4)#6 | 27.49(11) |
| O(6)#1-Sr(2)-Ga(4)#6 | 69.14(14) |
| O(3)#3-Sr(2)-Ga(4)#6 | 59.47(11) |
| O(3)#5-Sr(2)-Ga(4)#6 | 91.47(14) |
| O(5)#7-Sr(2)-Ga(4)#6 | 123.59(9) |
| O(5)#8-Sr(2)-Ga(4)#6 | 164.52(14) |
| Ga(2)#9-Sr(2)-Ga(4)#6 | 106.25(5) |
| Ga(2)#10-Sr(2)-Ga(4)#6 | 131.31(8) |
| Ga(4)#3-Sr(2)-Ga(4)#6 | 89.45(7) |
| Ga(4)#5-Sr(2)-Ga(4)#6 | 111.95(10) |
| O(2)-Bi(1)-O(6)#6 | 87.80(17) |
| O(2)-Bi(1)-O(6)#1 | 87.80(17) |
| O(6)#6-Bi(1)-O(6)#1 | 88.9(3) |
| O(2)-Bi(1)-Sr(1) | 170.54(17) |
| O(6)#6-Bi(1)-Sr(1) | 85.45(13) |

| | |
|---|---|
| O(6)#1-Bi(1)-Sr(1) | 85.45(13) |
| O(2)#9-Ga(1)-O(2) | 179.999(3) |
| O(2)#9-Ga(1)-O(5)#11 | 82.54(19) |
| O(2)-Ga(1)-O(5)#11 | 97.46(19) |
| O(2)#9-Ga(1)-O(5)#12 | 97.46(19) |
| O(2)-Ga(1)-O(5)#12 | 82.54(19) |
| O(5)#11-Ga(1)-O(5)#12 | 94.1(3) |
| O(2)#9-Ga(1)-O(5)#13 | 82.54(19) |
| O(2)-Ga(1)-O(5)#13 | 97.46(19) |
| O(5)#11-Ga(1)-O(5)#13 | 85.9(3) |
| O(5)#12-Ga(1)-O(5)#13 | 179.999(1) |
| O(2)#9-Ga(1)-O(5)#14 | 97.46(19) |
| O(2)-Ga(1)-O(5)#14 | 82.54(19) |
| O(5)#11-Ga(1)-O(5)#14 | 179.999(1) |
| O(5)#12-Ga(1)-O(5)#14 | 85.9(3) |
| O(5)#13-Ga(1)-O(5)#14 | 94.1(3) |
| O(2)#9-Ga(1)-Ga(2)#15 | 43.00(12) |
| O(2)-Ga(1)-Ga(2)#15 | 137.00(13) |
| O(5)#11-Ga(1)-Ga(2)#15 | 39.93(13) |
| O(5)#12-Ga(1)-Ga(2)#15 | 93.19(12) |
| O(5)#13-Ga(1)-Ga(2)#15 | 86.81(12) |
| O(5)#14-Ga(1)-Ga(2)#15 | 140.07(13) |
| O(2)#9-Ga(1)-Ga(2) | 43.00(13) |
| O(2)-Ga(1)-Ga(2) | 137.00(13) |
| O(5)#11-Ga(1)-Ga(2) | 86.81(12) |
| O(5)#12-Ga(1)-Ga(2) | 140.07(13) |
| O(5)#13-Ga(1)-Ga(2) | 39.93(13) |
| O(5)#14-Ga(1)-Ga(2) | 93.19(12) |
| Ga(2)#15-Ga(1)-Ga(2) | 62.92(3) |
| O(2)#9-Ga(1)-Ga(2)#9 | 137.00(13) |
| O(2)-Ga(1)-Ga(2)#9 | 43.00(13) |
| O(5)#11-Ga(1)-Ga(2)#9 | 93.19(12) |
| O(5)#12-Ga(1)-Ga(2)#9 | 39.93(13) |
| O(5)#13-Ga(1)-Ga(2)#9 | 140.07(13) |
| O(5)#14-Ga(1)-Ga(2)#9 | 86.81(12) |
| Ga(2)#15-Ga(1)-Ga(2)#9 | 117.08(3) |
| Ga(2)-Ga(1)-Ga(2)#9 | 180.0 |
| O(2)#9-Ga(1)-Ga(2)#10 | 137.00(12) |
| O(2)-Ga(1)-Ga(2)#10 | 43.00(13) |
| O(5)#11-Ga(1)-Ga(2)#10 | 140.07(13) |
| O(5)#12-Ga(1)-Ga(2)#10 | 86.81(12) |
| O(5)#13-Ga(1)-Ga(2)#10 | 93.19(12) |
| O(5)#14-Ga(1)-Ga(2)#10 | 39.93(13) |
| Ga(2)#15-Ga(1)-Ga(2)#10 | 180.0 |
| Ga(2)-Ga(1)-Ga(2)#10 | 117.08(3) |
| Ga(2)#9-Ga(1)-Ga(2)#10 | 62.92(3) |
| O(5)#16-Ga(2)-O(5)#13 | 168.7(3) |
| O(5)#16-Ga(2)-O(4)#17 | 93.85(19) |
| O(5)#13-Ga(2)-O(4)#17 | 94.00(19) |
| O(5)#16-Ga(2)-O(4)#14 | 94.00(19) |
| O(5)#13-Ga(2)-O(4)#14 | 93.85(19) |
| O(4)#17-Ga(2)-O(4)#14 | 91.9(3) |
| O(5)#16-Ga(2)-O(2)#2 | 81.4(2) |

O(5)#13-Ga(2)-O(2)#2 90.0(2)
O(4)#17-Ga(2)-O(2)#2 93.68(19)
O(4)#14-Ga(2)-O(2)#2 173.0(2)
O(5)#16-Ga(2)-O(2)#9 90.0(2)
O(5)#13-Ga(2)-O(2)#9 81.4(2)
O(4)#17-Ga(2)-O(2)#9 173.0(2)
O(4)#14-Ga(2)-O(2)#9 93.68(19)
O(2)#2-Ga(2)-O(2)#9 81.1(3)
O(5)#16-Ga(2)-Ga(1)#2 41.69(14)
O(5)#13-Ga(2)-Ga(1)#2 130.09(14)
O(4)#17-Ga(2)-Ga(1)#2 90.60(13)
O(4)#14-Ga(2)-Ga(1)#2 135.68(13)
O(2)#2-Ga(2)-Ga(1)#2 40.13(17)
O(2)#9-Ga(2)-Ga(1)#2 88.38(15)
O(5)#16-Ga(2)-Ga(1) 130.08(14)
O(5)#13-Ga(2)-Ga(1) 41.69(14)
O(4)#17-Ga(2)-Ga(1) 135.68(13)
O(4)#14-Ga(2)-Ga(1) 90.60(13)
O(2)#2-Ga(2)-Ga(1) 88.37(15)
O(2)#9-Ga(2)-Ga(1) 40.13(17)
Ga(1)#2-Ga(2)-Ga(1) 117.08(3)
O(5)#16-Ga(2)-Sr(2)#9 54.34(15)
O(5)#13-Ga(2)-Sr(2)#9 119.74(14)
O(4)#17-Ga(2)-Sr(2)#9 145.07(14)
O(4)#14-Ga(2)-Sr(2)#9 78.09(14)
O(2)#2-Ga(2)-Sr(2)#9 94.97(16)
O(2)#9-Ga(2)-Sr(2)#9 40.83(18)
Ga(1)#2-Ga(2)-Sr(2)#9 74.99(5)
Ga(1)-Ga(2)-Sr(2)#9 78.39(4)
O(5)#16-Ga(2)-Sr(2)#2 119.75(14)
O(5)#13-Ga(2)-Sr(2)#2 54.34(15)
O(4)#17-Ga(2)-Sr(2)#2 78.09(14)
O(4)#14-Ga(2)-Sr(2)#2 145.07(14)
O(2)#2-Ga(2)-Sr(2)#2 40.83(18)
O(2)#9-Ga(2)-Sr(2)#2 94.97(16)
Ga(1)#2-Ga(2)-Sr(2)#2 78.39(4)
Ga(1)-Ga(2)-Sr(2)#2 74.99(5)
Sr(2)#9-Ga(2)-Sr(2)#2 127.67(6)
O(5)-Ga(3)-O(6)#18 104.1(2)
O(5)-Ga(3)-O(3)#2 109.6(2)
O(6)#18-Ga(3)-O(3)#2 122.8(2)
O(5)-Ga(3)-O(4) 116.3(2)
O(6)#18-Ga(3)-O(4) 102.9(2)
O(3)#2-Ga(3)-O(4) 101.7(2)
O(5)-Ga(3)-Sr(2)#19 97.96(15)
O(6)#18-Ga(3)-Sr(2)#19 37.44(16)
O(3)#2-Ga(3)-Sr(2)#19 150.92(16)
O(4)-Ga(3)-Sr(2)#19 72.84(15)
O(5)-Ga(3)-Sr(2)#20 47.13(16)
O(6)#18-Ga(3)-Sr(2)#20 66.68(18)
O(3)#2-Ga(3)-Sr(2)#20 106.92(15)
O(4)-Ga(3)-Sr(2)#20 150.66(14)
Sr(2)#19-Ga(3)-Sr(2)#20 84.97(4)

| | |
|---|---|
| O(5)-Ga(3)-Sr(1) | 105.73(15) |
| O(6)#18-Ga(3)-Sr(1) | 149.84(17) |
| O(3)#2-Ga(3)-Sr(1) | 40.62(16) |
| O(4)-Ga(3)-Sr(1) | 67.28(14) |
| Sr(2)#19-Ga(3)-Sr(1) | 139.45(5) |
| Sr(2)#20-Ga(3)-Sr(1) | 134.95(4) |
| O(1)-Ga(4)-O(3) | 110.1(3) |
| O(1)-Ga(4)-O(6) | 104.2(3) |
| O(3)-Ga(4)-O(6) | 109.4(2) |
| O(1)-Ga(4)-O(4) | 107.2(2) |
| O(3)-Ga(4)-O(4) | 117.0(2) |
| O(6)-Ga(4)-O(4) | 108.1(2) |
| O(1)-Ga(4)-Sr(2)#5 | 92.3(2) |
| O(3)-Ga(4)-Sr(2)#5 | 46.93(16) |
| O(6)-Ga(4)-Sr(2)#5 | 72.74(19) |
| O(4)-Ga(4)-Sr(2)#5 | 159.20(15) |
| O(1)-Ga(4)-Sr(1)#10 | 66.9(3) |
| O(3)-Ga(4)-Sr(1)#10 | 48.33(16) |
| O(6)-Ga(4)-Sr(1)#10 | 140.76(18) |
| O(4)-Ga(4)-Sr(1)#10 | 111.04(14) |
| Sr(2)#5-Ga(4)-Sr(1)#10 | 69.68(6) |
| O(1)-Ga(4)-Sr(2)#1 | 67.3(3) |
| O(3)-Ga(4)-Sr(2)#1 | 136.29(16) |
| O(6)-Ga(4)-Sr(2)#1 | 39.98(17) |
| O(4)-Ga(4)-Sr(2)#1 | 104.41(14) |
| Sr(2)#5-Ga(4)-Sr(2)#1 | 89.44(7) |
| Sr(1)#10-Ga(4)-Sr(2)#1 | 128.27(3) |
| O(1)-Ga(4)-Sr(1) | 36.4(2) |
| O(3)-Ga(4)-Sr(1) | 137.02(16) |
| O(6)-Ga(4)-Sr(1) | 106.18(16) |
| O(4)-Ga(4)-Sr(1) | 72.22(14) |
| Sr(2)#5-Ga(4)-Sr(1) | 128.16(3) |
| Sr(1)#10-Ga(4)-Sr(1) | 88.711(17) |
| Sr(2)#1-Ga(4)-Sr(1) | 67.50(5) |
| Ga(4)-O(1)-Ga(4)#21 | 121.5(4) |
| Ga(4)-O(1)-Sr(1) | 117.8(2) |
| Ga(4)#21-O(1)-Sr(1) | 117.8(2) |
| Ga(1)-O(2)-Ga(2)#9 | 96.9(2) |
| Ga(1)-O(2)-Ga(2)#10 | 96.9(2) |
| Ga(2)#9-O(2)-Ga(2)#10 | 98.9(3) |
| Ga(1)-O(2)-Bi(1) | 136.2(3) |
| Ga(2)#9-O(2)-Bi(1) | 110.9(2) |
| Ga(2)#10-O(2)-Bi(1) | 110.9(2) |
| Ga(1)-O(2)-Sr(2) | 145.8(3) |
| Ga(2)#9-O(2)-Sr(2) | 105.1(2) |
| Ga(2)#10-O(2)-Sr(2) | 105.1(2) |
| Bi(1)-O(2)-Sr(2) | 9.64(9) |
| Ga(4)-O(3)-Ga(3)#10 | 117.5(2) |
| Ga(4)-O(3)-Sr(2)#5 | 103.0(2) |
| Ga(3)#10-O(3)-Sr(2)#5 | 119.9(2) |
| Ga(4)-O(3)-Sr(1)#10 | 101.8(2) |
| Ga(3)#10-O(3)-Sr(1)#10 | 113.5(2) |
| Sr(2)#5-O(3)-Sr(1)#10 | 98.07(16) |

| | |
|---|---|
| Ga(4)-O(4)-Ga(3) | 109.9(2) |
| Ga(4)-O(4)-Ga(2)#22 | 127.0(2) |
| Ga(3)-O(4)-Ga(2)#22 | 118.3(2) |
| Ga(3)-O(5)-Ga(2)#19 | 135.1(3) |
| Ga(3)-O(5)-Ga(1)#19 | 113.8(2) |
| Ga(2)#19-O(5)-Ga(1)#19 | 98.4(2) |
| Ga(3)-O(5)-Sr(2)#20 | 105.2(2) |
| Ga(2)#19-O(5)-Sr(2)#20 | 92.45(17) |
| Ga(1)#19-O(5)-Sr(2)#20 | 108.44(18) |
| Ga(4)-O(6)-Ga(3)#18 | 130.8(3) |
| Ga(4)-O(6)-Bi(1)#1 | 112.7(2) |
| Ga(3)#18-O(6)-Bi(1)#1 | 116.2(2) |
| Ga(4)-O(6)-Sr(2)#1 | 112.5(2) |
| Ga(3)#18-O(6)-Sr(2)#1 | 116.6(2) |
| Bi(1)#1-O(6)-Sr(2)#1 | 7.00(5) |

Symmetry transformations used to generate equivalent atoms:

#1 -x+2,-y+2,-z+2 #2 x,y,z+1 #3 -x+2,y,-z+1
#4 x,-y+2,z+1 #5 -x+2,-y+2,-z+1 #6 -x+2,y,-z+2
#7 x-1/2,-y+3/2,z-1/2 #8 x-1/2,y+1/2,z-1/2
#9 -x+1,-y+2,-z+3 #10 x,y,z-1 #11 x-1/2,-y+3/2,z+1/2
#12 -x+3/2,-y+3/2,-z+5/2 #13 x-1/2,y+1/2,z+1/2
#14 -x+3/2,y+1/2,-z+5/2 #15 -x+1,-y+2,-z+4
#16 -x+3/2,y+1/2,-z+7/2 #17 x-1/2,y+1/2,z+3/2
#18 -x+5/2,-y+3/2,-z+3/2 #19 x+1/2,y-1/2,z-1/2
#20 x+1/2,y-1/2,z+1/2 #21 x,-y+2,z
#22 x+1/2,y-1/2,z-3/2

**Table 4.** Anisotropic displacement parameters ($A^2 \times 10^3$). The anisotropic displacement factor exponent takes the form:

$$-2\pi^2 [ h^2 a^{*2} U11 + ... + 2 h k a^* b^* U12 ]$$

| Atom | U11 | U22 | U33 | U23 | U13 | U12 |
|---|---|---|---|---|---|---|
| Sr(1) | 7(1) | 14(1) | 21(1) | 0 | 10(1) | 0 |
| Sr(2) | 11(1) | 9(1) | 21(1) | 0 | 6(1) | 0 |
| Bi(1) | 11(1) | 9(1) | 21(1) | 0 | 6(1) | 0 |
| Ga(1) | 7(1) | 4(1) | 5(1) | 0 | 4(1) | 0 |
| Ga(2) | 3(1) | 4(1) | 3(1) | 0 | 1(1) | 0 |
| Ga(3) | 4(1) | 6(1) | 3(1) | 0(1) | 0(1) | 0(1) |
| Ga(4) | 5(1) | 4(1) | 3(1) | 0(1) | 1(1) | 0(1) |
| O(1) | 14(3) | 3(3) | 29(4) | 0 | 14(3) | 0 |
| O(2) | 8(3) | 8(3) | 5(3) | 0 | 3(2) | 0 |
| O(3) | 18(2) | 7(2) | 4(2) | 0(2) | 3(2) | -5(2) |
| O(4) | 8(2) | 7(2) | 4(2) | 1(1) | -1(2) | -3(2) |
| O(5) | 13(2) | 6(2) | 4(2) | -1(2) | 3(2) | -2(2) |
| O(6) | 3(2) | 15(2) | 23(2) | -6(2) | -3(2) | 2(2) |